



UNIVERSITAT ROVIRA I VIRGILI

## CONTINUOUS-WAVE AND PASSIVELY Q-SWITCHED SOLID-STATE MICROCHIP LASERS IN THE NEAR-INFRARED

Josep Maria Serres Serres

**ADVERTIMENT.** L'accés als continguts d'aquesta tesi doctoral i la seva utilització ha de respectar els drets de la persona autora. Pot ser utilitzada per a consulta o estudi personal, així com en activitats o materials d'investigació i docència en els termes establerts a l'art. 32 del Text Refós de la Llei de Propietat Intel·lectual (RDL 1/1996). Per altres utilitzacions es requereix l'autorització prèvia i expressa de la persona autora. En qualsevol cas, en la utilització dels seus continguts caldrà indicar de forma clara el nom i cognoms de la persona autora i el títol de la tesi doctoral. No s'autoritza la seva reproducció o altres formes d'explotació efectuades amb finalitats de lucre ni la seva comunicació pública des d'un lloc aliè al servei TDX. Tampoc s'autoritza la presentació del seu contingut en una finestra o marc aliè a TDX (framing). Aquesta reserva de drets afecta tant als continguts de la tesi com als seus resums i índexs.

**ADVERTENCIA.** El acceso a los contenidos de esta tesis doctoral y su utilización debe respetar los derechos de la persona autora. Puede ser utilizada para consulta o estudio personal, así como en actividades o materiales de investigación y docencia en los términos establecidos en el art. 32 del Texto Refundido de la Ley de Propiedad Intelectual (RDL 1/1996). Para otros usos se requiere la autorización previa y expresa de la persona autora. En cualquier caso, en la utilización de sus contenidos se deberá indicar de forma clara el nombre y apellidos de la persona autora y el título de la tesis doctoral. No se autoriza su reproducción u otras formas de explotación efectuadas con fines lucrativos ni su comunicación pública desde un sitio ajeno al servicio TDR. Tampoco se autoriza la presentación de su contenido en una ventana o marco ajeno a TDR (framing). Esta reserva de derechos afecta tanto al contenido de la tesis como a sus resúmenes e índices.

**WARNING.** Access to the contents of this doctoral thesis and its use must respect the rights of the author. It can be used for reference or private study, as well as research and learning activities or materials in the terms established by the 32nd article of the Spanish Consolidated Copyright Act (RDL 1/1996). Express and previous authorization of the author is required for any other uses. In any case, when using its content, full name of the author and title of the thesis must be clearly indicated. Reproduction or other forms of for profit use or public communication from outside TDX service is not allowed. Presentation of its content in a window or frame external to TDX (framing) is not authorized either. These rights affect both the content of the thesis and its abstracts and indexes.



UNIVERSITAT  
ROVIRA I VIRGILI

## Continuous-wave and passively Q-switched solid-state microchip lasers in the near-infrared

JOSEP MARIA SERRES SERRES



DOCTORAL THESIS  
2017

UNIVERSITAT ROVIRA I VIRGILI

CONTINUOUS-WAVE AND PASSIVELY Q-SWITCHED SOLID-STATE MICROCHIP LASERS IN THE NEAR-INFRARED

Josep Maria Serres Serres

UNIVERSITAT ROVIRA I VIRGILI

CONTINUOUS-WAVE AND PASSIVELY Q-SWITCHED SOLID-STATE MICROCHIP LASERS IN THE NEAR-INFRARED

Josep Maria Serres Serres

**Josep Maria Serres Serres**

***Continuous-wave and passively Q-switched  
solid-state microchip lasers in the near-infrared***

***Doctoral thesis***

Supervised by:

**Prof. Magdalena Aguiló**

**Dr. Xavier Mateos**

Doctoral Programme in Nanoscience, Materials and Chemical Engineering

Departament de Química Física i Inorgànica

Física i Cristal·lografia de Materials i Nanomaterials (FiCMA-FiCNA)



UNIVERSITAT ROVIRA I VIRGILI

**Tarragona 2017**

# **Continuous-wave and passively Q-switched solid-state microchip lasers in the near-infrared**

Josep Maria Serres Serres

© Josep Maria Serres Serres, 2017

Física i Cristal·lografia de Materials i Nanomaterials (FICMA - FICNA)

Departament de Química Física i Inorgànica

Universitat Rovira i Virgili

Tarragona, Spain



UNIVERSITAT  
ROVIRA I VIRGILI

DEPARTAMENT DE QUÍMICA FÍSICA  
I INORGÀNICA

Campus Sescelades  
Marcel·lí Domingo, s/n  
43007 Tarragona  
Tel. +34 977 55 81 37  
Fax +34 977 55 95 63  
www.quimica.urv.es

Prof. Dra. Magdalena Aguiló, Catedràtica de Cristal·lografia i Mineralogia, i Dr. Xavier Mateos, Professor Agregat, del Departament de Química Física i Inorgànica de la Universitat Rovira i Virgili,

**FEM CONSTAR,**

que aquest treball, titulat **Continuous-wave and passively Q-switched solid-state microchip lasers in the near-infrared**, que presenta **Josep Maria Serres Serres** per a l'obtenció del títol de Doctor, ha estat realitzat sota la nostra direcció al **Departament de Química Física i Inorgànica** d'aquesta universitat.

**Tarragona, 04/09/2017**

**Prof. Dra. Magdalena Aguiló**

**Dr. Xavier Mateos**

UNIVERSITAT ROVIRA I VIRGILI  
CONTINUOUS-WAVE AND PASSIVELY Q-SWITCHED SOLID-STATE MICROCHIP LASERS IN THE NEAR-INFRARED  
Josep Maria Serres Serres

# Abstract

## ***Continuous-wave and passively Q-switched solid-state microchip lasers in the near-infrared***

– Josep Maria Serres Serres –

This text discusses the characterization of compact solid-state lasers, as a first approach to the study of the microchip laser concept applied to several rare earth-doped crystalline hosts, and reports the results of studying the thermal lens required for microchip laser operation and continuous wave and passive Q-switched laser operation in microchip configuration.

In the experiments, the microchip concept is defined as a quasi-monolithic laser cavity. This concept is studied for laser emissions at  $\sim 1.06 \mu\text{m}$  from  $\text{Yb}^{3+}$  and  $\text{Nd}^{3+}$  ions, at  $\sim 1.3 \mu\text{m}$  from  $\text{Nd}^{3+}$ , at  $\sim 1.95 \mu\text{m}$  from  $\text{Tm}^{3+}$  and at  $\sim 2.05 \mu\text{m}$  from  $\text{Ho}^{3+}$ .

The continuous wave regime is examined in detail for the above mentioned trivalent lanthanide ions embedded in several crystalline hosts with the aim of comparing the potential of each gain material. In addition, the pump sources used depend on the needs of each laser material. Slope efficiencies attained in this study are very close to the theoretical limit improved by the quantum defect.

Microchip solid state lasers passively Q-switched with several saturable absorbers are also discussed. For this purpose, novel nanomaterials such as  $\text{MoS}_2$ , carbon nanostructures (SWCNTs, single- and multi-layer graphene) and SESA are used as saturable absorbers. Besides, the most conventional  $\text{Cr:YAG}$  ( $\sim 1.06 \mu\text{m}$ ) and  $\text{Cr:ZnS}$  ( $\sim 1.9 \mu\text{m}$ ) are examined and compared.

**Keywords:** Microchip lasers, Diode-pumped, Thermo-optic effects, Laser materials, Q-switched laser, Saturable Absorber.



# Preface

This PhD thesis was carried out within the research group Physics and Crystallography of Materials and Nanomaterials (FiCMA – FiCNA), of the Department of Physical and Inorganic Chemistry of the Universitat Rovira i Virgili (URV), Tarragona, Spain, between December 2013 and February 2017. It was supervised by Dr. Magdalena Aguiló and Dr. Xavier Mateos.

The study has been made possible by the financial support provided by the Spanish Ministry of Education and Science (MEC) under projects MAT2011-29255-C02-02, MAT2013-47395-C4-4-R, MAT2016-75716-C2-1-R and TEC2014-55948-R and by the Catalan Government's Department of Universities, Research and Information Society under projects 2009SGR235 and 2014SGR1358. I would like to acknowledge the personal financial support from the Universitat Rovira i Virgili under the project 2013PIPF-04-30 and the funding received by the European Union's Horizon 2020 research and innovation programme under grant agreement no 654148 Laserlab-Europe for mobility.

The research has been carried out in collaboration with several international research groups:

- Dr. Valentin Petrov and Dr. Uwe Griebner at the Max-Born Institute for Nonlinear Optics and Short Pulse Spectroscopy (Berlin, Germany),
- Dr. Pavel Loiko at the ITMO University (Saint Petersburg, Russia),
- Dr. Venkatesan Jambunathan, Dr. Antonio Lucianetti and Dr. Tomas Mocek at the HILASE Center, Institute of Physics ASCR (Dolní Brezany, Czech Republic),
- Prof. Konstantin Yumashev and Prof. Nikolai Kuleshov at the Center for Optical materials and Technologies, Belarusian National Technical University (Minsk, Belarus),
- Dr. Aleksei Onushchenko at the Vavilov State Optical Institute (Saint Petersburg, Russia),

- Prof. Huaijin Zhang at the State Key Laboratory of Crystal Materials, Shandong University (Jinan, China),
- Dr. Junhai Liu at the College of Physics, Qingdao University (Qingdao, China),
- Dr. J.I. Mackenzie at the Optoelectronics Research Centre, University of Southampton (Southampton, UK),
- Prof. Fabian Rottermund at the KAIST (Daejeon, Republic of Korea),
- Dr. Christian Kränkel at the University of Hamburg (Hamburg, Germany),
- Dr. Joan Rosell at the Droplets, IntErfaces, & FloWs (DEW), Universitat Rovira i Virgili (Tarragona, Spain),
- Dr. Arkady Major at the University of Manitoba (Winnipeg, Canada),
- Dr. Mauro Tonelli and Dr. Stefano Veronesi at the NEST Istituto Nanoscienze-CNR (Pisa, Italy) and
- Prof. Jiang Li at the CAS Shanghai Institute of Ceramics (Shanghai, China)

I am very pleased to have been able to work in several of these institutions (more specifically, MBI, HILASE and the DEW research laboratory) and to have worked in close contact with all these excellent people. Without their contribution, I could not have written this thesis.

Josep Maria Serres Serres  
Tarragona, 2017

# Acknowledgments

*Never consider the study as a duty, but as an opportunity to enter the beautiful and wonderful world of knowledge "Albert Einstein"*

Aquesta tesi doctoral no hauria estat possible sense l'ajuda, tant personal com professional, de moltes persones pròximes a mi, les quals m'han permès arribar al final d'aquesta primera etapa i tancar-la amb èxit, com investigador. És una satisfacció poder agrair, almenys de forma breu, a tots ells.

Primer de tot m'agradaria agrair sincerament al Prof. Francesc Díaz per acceptar-me al grup de recerca FICMA-FICNA, primerament per la realització del Treball de Màster i després per donar-me l'oportunitat d'iniciar els meus estudis de doctorat.

Aquest treball ha estat possible gràcies a la supervisió i dedicació dels meus directors de tesi, la Prof. Magdalena Aguiló i el Dr. Xavier Mateos al qual estic completament agraït pel seu ensenyament rebut al llarg d'aquest temps. No tinc paraules d'agraïment al Dr. Xavier Mateos per tot el temps invertit, paciència, amistat, ajuda i aprenentatge rebut. Davant de totes les dificultats sempre ha estat el més a prop possible per poder-me donar un cop de mà o simplement escoltar-me en els moments que ho necessitava, tant en l'àmbit professional com personal.

M'agradaria agrair als membres sèniors del que es compon el grup FICMA-FICNA, Dr. Jaume Massons, Dra. Maria Rosa Solé, Dra. Cinta Pujol i Dr. Joan Josep Carvajal els quals en algun moment, de forma desinteressada, m'han pogut donar consells i/o recomanacions per tirar endavant el projecte. També el Dr. Arian Ródenas que durant un temps en va formar part del grup de recerca. En especial, vull agrair al Dr. Joan Josep Carvajal i paral·lelament al Dr. Joan Rosell, del grup DEW, per l'aprenentatge, treball i intensa dedicació rebuda durant el meu primer any dins del grup.

I would like to thank Dr. Uwe Griebner and Dr. Valentin Petrov for giving me the opportunity to work at MBI, Berlin, Germany as well as, Dr. Tomas Mocek and Dr. Antonio

Lucianetti to accept me to work at HILASE, Dolní Brezany, Czech Republic. Last but not least, it was a pleasure to work, in the laboratory, with Dr. Venkatesan Jambunathan and Dr. Pavel Loiko by their motivation, constant support, knowledge and friendship.

Agrair el treball realitzat per part dels tècnics, a l'Ernest Arce per preparar-me suports per la cavitat làser, a Lukas, Merce, Mariana, Rita, Núria, F. Xavier del SRCIT de la URV per ajudar-me en la caracterització de mostres, i en especial als tècnics de FICMA - FICNA, Agustí Montero, Nicole Bakker i a les ex-tècniques, Gemma Marsal i Laura Escorihuela per preparar-me mostres, aconsellar-me i fer possible el treball diari en el laboratori.

A tots els companys, del grup FICMA-FICNA, Oleksandr Bilousov, Oleksandr Savchuk, Ali Butt, Eric Pedrol, Marc Medina, Josue Mena, Irina Adell, Huu Dad Nguyen, Javier Martinez, Esrom Kifle, Xhuzao Zhang i als companys del grup DEW Nikolas Sochorakis i Eszter Bodnár pel seu companyerisme i amistat durant aquest temps que hem compartit junts.

No em vull oblidar del company Víctor Grau que ha fet més portadora aquesta etapa tant dins com fora de la universitat en l'amistat personal, paciència, xerrades, dinars i llargs cafès. Gràcies pel reforç emocional i consells per com continuar endavant i fer-me pensar amb altres alternatives.

Vull agrair a tota la meva família pel seu suport i paciència, especialment als meus pares que amb els alts i baixos sempre m'han animat a continuar, i amb especial èmfasi a la meva nova família, Romina i Edurne, ja que no he pogut estar tot el temps desitjat i necessari per a la seva atenció i dedicació. Tot i així, al llarg d'aquesta etapa personal, han estat incondicionalment al meu costat. Gràcies, per estar en cada moment al meu costat.

*Per a Romina i Edurne*



# Table of Contents

<b>Abstract</b> .....	i
<b>Preface</b> .....	iii
<b>Acknowledgments</b> .....	v
<b>1. Motivation for the work</b> .....	1
<b>2. Introduction</b> .....	5
2. 1. Microchip Lasers .....	6
2. 2. Host materials .....	7
2. 3. Rare-Earth ions .....	8
2. 4. Thermal lens .....	10
2. 5. Q-switching mechanism .....	14
2. 6. Passive Saturable Absorbers .....	16
<b>3. Objectives</b> .....	19
<b>4. Results</b> .....	21
4. 1. Continuous-wave laser operation .....	22
4. 2. Thermal lens .....	28
4. 3. Passively Q-switched laser operation .....	31
<b>5. Conclusions</b> .....	35
<b>6. Appendix</b> .....	41
6.1 Pump sources .....	42
6.2 Optical elements .....	44
6.3 Crystal holders for cooling .....	45
6.4 Cavity setups .....	46
6.5 External devices .....	47
6.6 Electrospinning setup .....	48
6.7 Growth, cutting and polishing crystals .....	48
6.8 Spectroscopic characterization .....	49
6.9 Microscopic techniques .....	49
<b>References</b> .....	51
<b>List of Publications</b> .....	59

UNIVERSITAT ROVIRA I VIRGILI  
CONTINUOUS-WAVE AND PASSIVELY Q-SWITCHED SOLID-STATE MICROCHIP LASERS IN THE NEAR-INFRARED  
Josep Maria Serres Serres

1.

# Motivation for the work

In less than 60 years, the word “laser” has changed from being associated with popular science fiction, with big monsters emitting light from their eyes, to having real scientific applications in our daily lives. Since the first demonstration of lasers using a synthetic ruby in the 1960s all classes of lasers have developed at great speed [1, 2]. The number of scientific reports has increased exponentially and have explored new materials, pump schemes, temporal regimes, wavelengths, applications, etc. Emerging companies have started to commercialize different kinds of these novel lasers and have found a multitude of applications in medicine, the military, micromachining, automobile engines, scientific development, and many other fields. In solid-state lasers, SSL, emerging active ions (transition metals or rare-earths) are divalent ( $\text{Sm}^{2+}$ ,  $\text{Dy}^{2+}$ ,  $\text{Tm}^{2+}$ ,  $\text{Ni}^{2+}$ ,  $\text{Co}^{2+}$  and  $\text{V}^{2+}$ ) or trivalent ( $\text{Nd}^{3+}$ ,  $\text{Er}^{3+}$ ,  $\text{Ho}^{3+}$ ,  $\text{Ce}^{3+}$ ,  $\text{Tm}^{3+}$ ,  $\text{Pr}^{3+}$ ,  $\text{Gd}^{3+}$ ,  $\text{Eu}^{3+}$ ,  $\text{Yb}^{3+}$  and  $\text{Cr}^{3+}$ ) [3-9]. These can generate light in different regions of the electromagnetic spectrum, from ultraviolet to mid-infrared. In former times, it was only possible to achieve a few milli-watts of output power but the new pump systems and improved materials have helped to achieve multi-watt operation. The new powerful semiconductor laser

diodes (LDs) can be used to explore the limits of solid-state materials, and to investigate, improve and achieve optimal optical-to-optical light conversions for the optical, mechanical and thermal properties of each active medium [10].

Thanks to the new pumped sources developed, high efficiency, reliability, flexibility and compactness can be achieved at several laser wavelengths, which makes it possible to study such new doped-crystals (laser materials) as garnets, sesquioxides, borates, vanadates, fluorides, monoclinic double tungstates (MDTs), and explore the combination of dopant and host that is most suited to the desired application. Cubic crystals, such as garnets or sesquioxides, are very attractive SSL materials because of their simple crystalline structure, high thermal conductivity and small thermal expansion, among other properties [11-14]. They are well known, and have been studied and commercialized. Neodymium-doped YAG is the most common laser in research and commercial applications emitting at 940, 1120, 1064 and 1440 nm in CW and pulsed regime. Besides, it is frequency doubled or tripled. With the same host, other ions ( $\text{Yb}^{3+}$ ,  $\text{Er}^{3+}$ ,  $\text{Tm}^{3+}$  and  $\text{Ho}^{3+}$ ) have been studied in the range 1 and 3  $\mu\text{m}$  and have been found to perform well. As an example, the Yb:YAG in thin-disk geometry is the most promising laser material operating at 1  $\mu\text{m}$  for power scaling purposes [15-17].

The practical focus of this study is the emissions at  $\sim 1 \mu\text{m}$  ( $\text{Yb}^{3+}$  and  $\text{Nd}^{3+}$ ),  $\sim 1.3 \mu\text{m}$  ( $\text{Nd}^{3+}$ ) and  $\sim 2 \mu\text{m}$  ( $\text{Tm}^{3+}$  and  $\text{Ho}^{3+}$ ) from several crystalline hosts as laser materials. These lasers can potentially be applied in deontology, laser ignition, material processing, range finding, surgery and hair removal (at  $\sim 1 \mu\text{m}$ ,  $\sim 1.3 \mu\text{m}$ ) and in spectroscopy, LIDAR, tissue ablation, kidney stone removal and atmospheric applications (at  $\sim 2 \mu\text{m}$ ) [18-26]. For this purpose, we study not only laser performance but also several properties (thermal and optical) to optimize the laser parameters. Comparing the ions in various crystals gives more detail about such laser parameters as wavelength, tuning range, crystal fracture, optical-to-optical efficiency, maximum output power, etc.

Laser generation can be either in continuous-wave (CW) or pulsed mode. Of the different ways to generate laser pulses, the so-called Q-switched technique generates short and very energetic laser pulses with practical applications in the real world [18, 19, 27-29]. This

technique can be either active or passive. The active materials that generate pulses modulate the intensity of the laser oscillating in the cavity and convert acoustic, electric or mechanical modulation to optical modulation [30-33]. A second way to generate laser pulses is passive Q-switching (PQS), which uses passive materials (namely saturable absorbers [SAs]) for optical modulation [34-37]. The most common SAs are the Cr:YAG crystal for lasers at 1  $\mu\text{m}$  and Cr:ZnSe for lasers at 2  $\mu\text{m}$  [38,39]. In recent years, huge efforts have been made to explore new SAs based in nanomaterials to improve the generation of laser pulses. Good examples are those SAs based on carbon nanostructures, such as graphene, single- or multi-walled carbon nanotubes (SWCNTs, MWCNTs), etc. [40-43]. These materials have very fast recovery times, low saturation intensities, and high damage thresholds while their modulation depth is somehow “customized” (for example, by controlling the concentration of SWCNTs the modulation depth can also be controlled [44-47]).

The laser cavity geometry plays an important role in achieving the desirable output results: devices are required to be economic to fabricate, reliable, alignment-free, simple, compact and robust. One laser cavity that can provide these results is the microchip concept. The microchip laser setup consists of a plano-plano cavity with optical coatings deposited directly on the active material. This concept can be applied in both CW and PQS [28, 29, 48-53]. Novel nanomaterials can be deposited directly on the active materials and then be covered with a specific dielectric mirror to generate laser oscillation at the proper wavelength. The most important feature of the microchip laser concept is the thermo-optical properties of the laser material. Due to the geometry of the laser cavity (two planar mirrors), the laser mode needs to be stabilized by introducing a focusing element. This is provided by the laser material itself if it has a positive thermal lens (TL). In addition, if the TL is weak, the astigmatism will be weak and the laser beam will be quasi circular with good quality factor at high absorbed power.

In this thesis, the microchip lasers studied, either CW or pulsed, are intended to operate at 1, 1.3 and 2  $\mu\text{m}$ .





# *I*ntroduction

2. 1. Microchip Lasers .....	6
2. 2. Host materials .....	7
2. 3. Rare-Earth ions .....	8
2. 4. Thermal lens .....	10
2. 5. Q-switching mechanism.....	14
2. 6. Passive Saturable Absorbers.....	16

This second chapter gives an overview of some of the most important issues associated with SSLs. The mechanism and the advantages of microchip lasers are discussed (2.1). The thermal, optical and mechanical properties of several host materials (2.2) are overviewed and the active ions studied ( $\text{Yb}^{3+}$ ,  $\text{Nd}^{3+}$ ,  $\text{Tm}^{3+}$  and  $\text{Ho}^{3+}$ ) are described (2.3). The TL is a key parameter for understanding the mechanism of mode stabilization in the plan-parallel configuration of the laser cavity (2.4). The Q-switching mechanism that produces short and high energetic laser pulses is also explained (2.5) and, finally, the main properties of the SAs for generating laser pulses are shown (2.6).

## 2. 1. *Microchip Lasers*

SSLs are assembled with discrete optical components, most of which need to be carefully aligned. This generally makes them expensive, fragile and unattractive for many commercial and scientific applications. Emerging SSLs were rapidly developed thanks to the advances made in pump sources, especially semiconductors because they cover the absorption band of most transition metals and rare-earth ions [54-58]. The cost per watt was quickly decreased by low-cost mass production, simple setup, robustness, compactness and inexpensive automation, and many regions of the electromagnetic spectrum were also covered. Two decades ago, the MIT Lincoln Laboratory built a novel device called “a microchip laser” to overcome the problems of cost, robustness, reliability and size [48-51]. This concept of laser consists of a thin active material with dielectric coatings/mirrors directly applied to its plane surfaces to form a “sandwich” in the laser resonator. With this concept, many applications changed from being “unattractive” to “attractive”.

End-pumped microchip lasers offer advantages such as high-power efficiency, simplicity, robustness and compactness with moderate output powers [59]. Moreover, diode pumped microchip SSLs offer a such advantages as high beam quality, small linewidth, output stability (amplitude noise is typically below <1%), high energy pulses (the upper state lifetime of most of the active ions can exceed several hundred microseconds, which makes them attractive for Q-switching) [60-64]. The main disadvantage of this type of laser resonator, in which the gain medium is longitudinally pumped, is the temperature dependence along the beam direction [65]. The absorption of the pump produces thermal gradients that directly affect the refractive index of the laser material, which makes the thermo-optic coefficients govern the laser mode. These thermo-optic coefficients are key to the stability of the laser mode in this plan-parallel resonator because they affect the beam quality. The microchip concept can be applied in CW, PQS and the self-mode-locking with excellent performance. It also makes it possible to fabricate frequency-doubled lasers and Raman lasers, etc.

## 2. 2. Host materials

The active material in a laser consists of a host and the ion. The former is a passive element, while the absorption and emission processes take place in the active ions depending on distribution of their energy levels (see 2.3).

The passive behaviour of the host induces the mechanical, optical and thermal properties of the laser material (see Table 2). Ideally it should have high thermal conductivity, low thermal expansion coefficients, low mechanical-thermal stress, a high damage threshold, limited scatter loss and hardness. It is important that the quality of the active materials (host + active ions) be high if laser performance is to be good. When the active ions substitute a passive ion in the structure, the crystallinity of the laser materials should not be affected too much [66-70]. As for the active ions, they must have strong absorption bands and high quantum efficiency in the emission process. In this thesis, the active ions studied are Yb, Nd, Tm and Ho embedded in several hosts. Table 1 shows how the ionic radius affects the suitability of the active ions to substitute for passive ions. The table shows the ionic radius that depends on the coordination in the structure of the active ion substituting the passive ion. The coordination depends on the host (VI or VIII as an example).

**Table 1.** List of RE with the substituted active to passive atom in the host. #\* bests radii-matching

Passive/Active ionic radii		ACTIVE ION			
		Yb	Nd	Tm	Ho
PASSIVE ION	Lu	0,9883*	0,8522	0,9758*	0,9412
	Y	1,0489*	0,9045	1,0357*	0,9989*
	Gd	1,0932	0,9477*	1,079	1,0411*
	Sc	0,8683	0,7487	0,8573	0,8269
	Mg	0.8392	0.7236	0.8285	0.7991
	Na	1.1888	1.025*	1.1738	1.1321

The materials studied are classified as isotropic and anisotropic materials. The isotropic ones are crystals that have the same refractive index in all optical directions [71]. In these groups, we find garnets, spinels, sesquioxides and others. Hence, the anisotropic crystals are divided into uniaxial and biaxial crystals, which are those whose refractive index depends on the direction of the light propagation [71]. Here, fluorides and MDTs are found, among others.

### 2.3. Rare-Earth ions

Rare-earth ions are commonly used for laser applications [10, 18, 72, 73]. They are located in the periodic table of the elements after lanthanum. The group of lanthanides has the electronic configuration  $[\text{Xe}] 6s^2 5d^0 4f^n$  (where  $n$  is the number of 4f electrons from  $0 < n < 14$ , but La, Ce, Gd and Lu exceptionally have  $5d^1$  instead of  $5d^0$ ). Lanthanides are commonly incorporated as trivalent cations. In this oxidation state, the electronic configuration is  $[\text{Xe}] 4f^n$  (see Table 3). The electrons are only filled in the 4f shell, and the electrons in the 6s and 5d shells are lost. In fact, the valence electrons are responsible for their absorption/emission transitions.

**Table 3.** The number of 4f electrons ( $n$ ) in the 3+ oxidation state

Ion	La <sup>3+</sup>	Ce <sup>3+</sup>	Pr <sup>3+</sup>	Nd <sup>3+</sup>	Pm <sup>3+</sup>	Sm <sup>3+</sup>	Eu <sup>3+</sup>	Gd <sup>3+</sup>	Tb <sup>3+</sup>	Dy <sup>3+</sup>	Ho <sup>3+</sup>	Er <sup>3+</sup>	Tm <sup>3+</sup>	Yb <sup>3+</sup>	Lu <sup>3+</sup>
n	0	1	2	3	4	5	6	7	8	9	10	11	12	13	14

The *Ytterbium* ion is the simplest system because only one excited state is possible corresponding to the  $^2F_{7/2} \rightarrow ^2F_{5/2}$  transition. At room temperature, this correspond to a quasi-4-level laser system. The absorption broadband for Yb<sup>3+</sup> is between 880-1000 nm depending on the host [74-77]. This in-band pumping system shows very efficient the laser generation, reducing the fractional heat load (low losses by no-radiative processes) and very low quantum defect (<10%) providing high slope efficiencies and high optical-to-optical conversions. The simple energy level scheme avoids the up-conversion (UC) and the excited-state absorption (ESA processes).

The *Neodymium* ion is a 4-level laser system that can be pumped at ~808 nm. The studied emissions correspond to the of  $^4F_{3/2} \rightarrow ^4I_{11/2}$  transition at ~1067 nm and the  $^4F_{3/2} \rightarrow ^4I_{13/2}$  transition at ~1350 nm. The pure 4-level laser systems present a very low threshold ( $^4I_{9/2}$  is the ground state) and high optical-to-optical laser efficiency [78-82].

Properties	Double tungstate (KLuW)	Garnet (YAG)	Sesquioxide (Lu <sub>2</sub> O <sub>3</sub> )	Vanadate (LuVO <sub>4</sub> )	Fluoride (YLF)	Oxyborate (YCOB)	Borate (YAB)	Aluminate (CALGO)	Tungstate (MgWO <sub>4</sub> )	
<b>Crystal system</b>	monoclinic	Cubic	Cubic	Tetragonal	Tetragonal	Monoclinic	Trigonal	Tetragonal	Monoclinic	
<b>Refractive index @1 μm</b>	Ng = 2.084	1.842	1.911	n <sub>o</sub> = 1.998	n <sub>o</sub> = 1.448	X = 1.657	n <sub>o</sub> = 1.758	n <sub>o</sub> = 1.925	X = 2.1255	
	Nm = 2.030			n <sub>e</sub> = 2.234	n <sub>e</sub> = 1.470	Y = 1.688	n <sub>e</sub> = 1.688	n <sub>e</sub> = 1.941	Y = 2.1400	
	Np = 1.995			Z = 1.698	Z = 2.2731					
<b>Refractive index @2 μm</b>	Ng = 2.05	1.813	1.896	n <sub>o</sub> = 1.975	n <sub>o</sub> = 1.442	X = 1.654	n <sub>o</sub> = 1.754	n <sub>o</sub> = 1.905	X = 2.1047	
	Nm = 1.99			n <sub>e</sub> = 2.158	n <sub>e</sub> = 1.464	Y = 1.686	n <sub>e</sub> = 1.684	n <sub>e</sub> = 1.924	Y = 2.1182	
	Np = 1.94			Z = 1.696	Z = 2.2455					
<b>Hardness (Mohs scale)</b>	4 - 5.5	8.2 - 8.5	7	5	4 - 5	6 - 6.5	7.5	8	4.5	
<b>Transparency range (nm)</b>	365 - 5110	200 - 6000	350 - 5500	450 - 5000	200 - 6700	210 - 2600	Not found	Not found	400 - 4000	
<b>Space group/ Class</b>	C2/c - 2/m	la3d	la3	I4 <sub>1</sub> /amd	I4 <sub>1</sub> /a	Cm	R32	I4/mmm	P2/c	
<b>Lattice parameters</b>	a = 1.0576 nm	a = 1.21 nm	a = 1.04 nm	a = 0.702 nm	a = 0.516 nm	a = 0.8077 nm	a = 0.9293 nm	a = 0.3663 nm	a = 0.4697 nm	
	b = 1.0214 nm			b = 1.6019 nm	b = 1.6019 nm	a = 0.9293 nm	a = 0.3663 nm	b = 0.5678 nm		
	c = 0.7487 nm			c = 0.629 nm	c = 1.074 nm	c = 0.7245 nm	c = 1.2010 nm	c = 0.4933 nm		
	B = 130.68°			B = 90°	B = 90°	B = 90°	B = 101.17°	B = 90°	B = 90°	B = 90.77°
	Z = 4			Z = 8	Z = 16	Z = 4	Z = 4	Z = 2	Z = 3	Z = 4
<b>Unit cell volume (nm<sup>3</sup>)</b>	0.6133	1.73	1.11	0.307	0.286	0.434	0.625	0.162	0.13154	
<b>Density (g/cm<sup>3</sup>)</b>	7.69	4.56	9.42	6.26	3.95	3.31	3.7	5.97	6.89	
<b>Thermal conductivity @298K (W/mK)</b>	K <sub>1</sub> = 3.09	13	12.2	a = 11	a = 5.3	a <sub>x</sub> = 2.6	4.7 (arbitrary orientation)	a = 6.9	8.7 (arbitrary orientation)	
	K <sub>2</sub> = 2.55			c = 4.4	c = 7.2	a <sub>y</sub> = 2.33		c = 6.3		
	K <sub>3</sub> = 4.4			a <sub>z</sub> = 3.1						
<b>Thermal Expansion α (10<sup>-6</sup>K<sup>-1</sup>)</b>	N <sub>g</sub> = 14.55	8	7.9	a = 4.4	a = 14.31	a <sub>x</sub> = 10.8	K <sub>a</sub> = 7.7	K <sub>a</sub> = 10	a = 10.47	
	N <sub>p</sub> = 11.19			c = 11	c = 10.05	a <sub>y</sub> = -8.8		K <sub>c</sub> = 16	K <sub>c</sub> = 16	b = 15.68
	N <sub>m</sub> = 3.35			a <sub>z</sub> = 3.4	c = 10.75					
<b>References</b>	70, 83, 84, 85, 86	86, 87, 88	86, 89, 90	86, 91, 92	86, 93, 94	86, 95, 96	86, 97, 98	86, 99, 100, 101	86, 102, 103, 104	

**Table 2.** Structural, optical, thermal and mechanical properties of the hosts studied

The thulium ion is one of the most suitable and efficient systems for lasers at 2  $\mu\text{m}$  due to the high quantum efficiency (>75% in the worst case) caused by the so-called cross-relaxation mechanism (CR), which reduces heat loading. The  $\sim 2 \mu\text{m}$  emission corresponds to the  $^3F_4 \rightarrow ^3H_6$  transition. The CR mechanism allows for 2 Tm ions to be excited to the  $^3F_4$  level with only one pump photon [105-108].

The holmium ion generates light at  $\sim 2.1 \mu\text{m}$  corresponding to the  $^5I_7 \rightarrow ^5I_8$  transition [109-111]. To reduce the fractional heat load, it is typically pumped at  $\sim 1.9 \mu\text{m}$ , directly to the upper laser level, providing highly efficient lasers.

Co-doped systems such as  $\text{Yb}^{3+} - \text{Tm}^{3+}$  or  $\text{Tm}^{3+} - \text{Ho}^{3+}$  are a possible alternative to the above ions. The first ion acts as a sensitizer of the emission of the second ion. The co-doped systems make it possible to use conventional laser diodes for pumping. However, the main drawback is the limited energy transfer efficiency between the ions, which limits the efficiency of the laser and the power scalability potential [112].

## 2. 4. Thermal lens

When light interacts with matter, heat is generated. This is basically due to the absorption of light because part of the absorbed energy is converted into lower energy photons (releasing less energy than is absorbed, and transferred to the host, thus increasing its temperature [113-114].

This thesis gives particular importance to thermo-optic effects because they are mainly responsible for limiting power scaling, modifying the refraction index, depolarization, altering the stability domains in the cavity, efficiency and the degradation of the quality of the laser beam. This is especially true in plan-plan cavities [115-116].

The TL phenomena are generated because of the non-uniform transversal and longitudinal temperature distribution in the active material [117]. The transverse gradient of the refractive index due to the hotter centre of the beam, together with the changes caused by thermally induced mechanical stress can lead to bulging at the end of the crystal faces. As is

well known, these contributions are dominated mainly by the thermal expansion and thermal conductivity coefficients, which depend on the active material.

At low absorbed power, the thermal effects are not significant. However, the thermal focal length changes with the absorbed power, meaning that the laser mode undergoes some changes. This can be corrected in long laser cavities with a curved mirror [118] by readjusting the position of the mirrors or using internal cavity lenses at a specific pump power. It is more of a problem in a plan-plan cavity because it is at the border of the mode stability ( $D = 0$ ) (see Fig. 1) A positive ( $D > 0$ ) or negative ( $D < 0$ ) sign means focusing or defocusing, respectively, which makes the configuration stable or unstable. A positive, focusing, thermal lens is required to keep the laser action within the stability region.

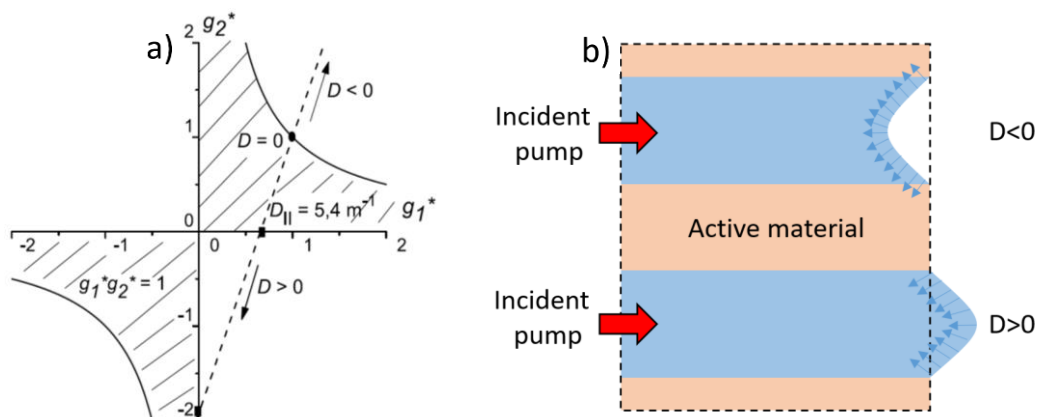


**Figure 1.** a) Diagram of the mode stability with positive or negative sign of  $D$  in a plan-plan laser cavity (reproduced from [119]) and b) Thermal aberrations in the active material

The thermo-optic coefficient is given by:

$$\Delta = \frac{dn}{dT} + P_{PE} + Q_{dist} \cdot \quad 2.1$$

In optical materials, the refractive index is not constant with temperature,  $\frac{dn}{dT}$ . The second factor is the photo-elastic effect,  $P_{PE}$ , which means that the refractive index depends on thermally induced stress. It depends on  $n^3 \alpha_T Q_{A(B)}$  where  $Q_{A(B)}$  is the so-called photo-

**Table 4.** Thermo-optic coefficients of several laser materials doped with Yb ions

Active material		$\frac{dn}{dt}$ $10^{-6}K^{-1}$	Ppe $10^{-6}K^{-1}$	Qdist $10^{-6}K^{-1}$	Ref.
<b>Yb:CALGO</b> (9 at.%Yb)	a-cut	-7.6	0 (E    a) -5.3 (E    c)	+8.9 (E    a) +14.2 (E    c)	<b>120, 121</b>
	c-cut	-8.6	-0.1 (E    a) /	+9.3 (E    a) /	
	Ng-cut	-6.5	+2.2 (E    m) +0.4 (E    p)	+13.3	
<b>Yb:KluW</b> (3 at.% Yb)	Np-cut	-6.5	+5.4 (E    m) -1.1 (E    g)	+3.4	<b>122, P3</b>
	Nm-cut	-14.6	+4.8 (E    g) -2.4 (E    p)	+11.0	
<b>Yb:YAG</b> (8 at.% Yb)	/	+9	-0.66	+7.2	<b>123, 124</b>
<b>Yb:Lu<sub>2</sub>O<sub>3</sub></b> (1.5 at.% Yb)		+5.8	Not found	+10.3	<b>123, 125</b>
<b>Yb:YVO4</b> (1 at.% Yb)	a-cut	+13.8	Not found	+3.5 (E    a) -3.4 (E    c)	<b>126, 127</b>
	c-cut	+8.0		+14 (E    a) /	
<b>Yb:YLF</b> (5 at.% Yb)	a-cut	-4.6	Not found	+6.41 (E    a) +6.7 (E    c)	<b>128, 129</b>
	c-cut	-6.6		+4.5 (E    a) /	
<b>Yb:YCOB</b> (15 at.% Yb)	X-cut	-2.5	-1.7 (E    Y) -1.2 (E    Z)	+10.6	<b>130, P18</b>
	Y-cut	-2.5	+1.9 (E    X) +3.4 (E    Z)	+2.3	
	Z-cut	-1.2	+1.9 (E    X) +1.1 (E    Y)	+4.9	
<b>Yb:YAB</b> (7 at.% Yb)	a - cut	+3.5	Not found	+1.2 (E    a) +1 (E    c)	<b>131</b>
	c - cut	+6.0		+6.5 (E    a) /	
<b>Yb:YALO</b> (5 at.% Yb)	a-cut	+7.7	Not found	+7.5 (E    b) +8.08 (E    c)	<b>132</b>
	b-cut	+11.7		+2.2 (E    a) +8.2 (E    c)	
	c-cut	+8.3		+2.2 (E    a) +7.7 (E    b)	

elastic constant. The last factor is the non-uniform expansion due to the thermal heat in the active media. This factor depends on the refractive index and the coefficient of the thermal expansion along the light propagation axis. The bulging of the crystal end faces is due to a non-uniform thermal expansion coefficient defined as  $Q_{dist} = (1 - \nu)(n - 1)\alpha_T$ . Table 4 shows the thermo-optic coefficient ( $dn/dT$ ,  $P_{pe}$  and  $Q_{dist}$ ) of several laser materials in the literature. These thermo-optic coefficients depend on the ion and the doping level.

For end-pumped bulk crystals the optical power of the TL can be determined as:

$$D = \frac{P_{abs} \cdot \eta_h}{2 \cdot \pi \cdot w_p^2 \cdot K} \Delta, \quad 2.2$$

where  $P_{abs}$  is the absorbed power in the crystal, and  $\eta_h$  is the fractional heat load, which is usually determined by  $1 - \lambda_p/\lambda_l$  where  $\lambda_p$  is the pump wavelength and  $\lambda_l$  the laser wavelength,  $w_p$  is the pump spot radius and  $K$  the thermal conductivity. In this study,  $w_p$  was considered to be higher than the radius incident pump so the beam quality is less influenced by thermally-induced aberrations. When  $w_p < w_l$ , the beam quality is degraded because of the wave-front distortion introduced by non-parabolic phase aberrations of the TL [133].

The dioptric power,  $M$ , is calculated as  $f^{-1} = D$ . Another factor that describes the changes in the optical power of TL with the absorbed power is the sensitivity factor. It is defined as:

$$M = \frac{d(1/f)}{dP_{abs}}, \quad 2.3$$

The difference in the sensitivity factors of the two meridional planes is the astigmatism, defined as:

$$S = M_v - M_H, \quad 2.4$$

where  $M_v$  or  $M_H$  are the sensitivity factors for the vertical and horizontal planes, respectively. The astigmatism degree evaluates the ellipticity of the laser beam.

## 2. 5. Q-switching mechanism

Q-switching is a mode of laser operation that provides short and energetic laser pulses. It modulates intracavity losses and thus the quality factor  $Q$  of the laser resonator. The latter is defined as the ratio of the energy stored in the cavity to the energy loss per cycle:

$$Q = E_{\text{stored}} / E_{\text{loss}} \quad 2.5$$

The technique consists of storing energy in the amplifying medium by optical pumping while preventing lasing. This is done by loss insertion, which increases the threshold. The energy stored and the gain of the active medium will be high.

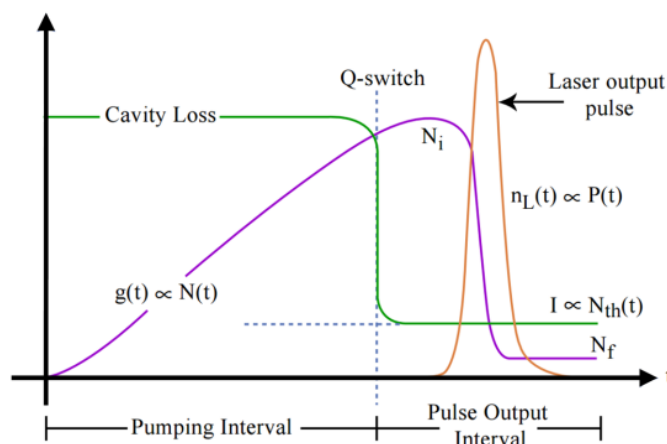


**Figure 2.** Evolution of power, loss and gain during the formation of a laser pulse with the Q-switching technique, reproduced from [134]

The time for which the atoms remain excited in the upper laser level depends on the fluorescence lifetime  $\tau_f$ . The longer this is, the better. For passive Q-switching the losses are modulated with an SA, an optical component with a certain optical loss, which is reduced at high optical intensities. It acts as a passive modulator, because it inserts a certain amount of losses in the cavity. When the optical intensity reaches a particular value, the losses are reduced, and a pulse is generated (see Figure 2). The pulse duration achieved with Q switching is typically in the nanosecond range or even shorter.

The main characteristics of a Q-Switched laser are the following: the pulse energy ( $E_p$ ), the repetition rate ( $f_{rep}$ ) and the pulse duration ( $t_p$ ). These values can be determined experimentally or modelled with theoretical formulas.

The pulse energy can be estimated as follows:

$$E_p = \frac{h\nu_L}{\sigma_L} \cdot A \cdot \Delta R \cdot \frac{T}{T+A_{ns}}, \quad 2.6$$

where  $h\nu_L$  is the photon energy at the lasing wavelength,  $\sigma_L$  the emission cross section of the laser material,  $A$  is the pump spot area in the resonator,  $\Delta R$  is the modulation depth of the SA,  $T$  is the transmission of the output coupler and  $A_{ns}$  is the non-saturable losses.

The repetition rate shows linear behaviour by changing the pump:

$$f_{rep} = \frac{P_{av}}{E_p} = \frac{\eta_s \cdot (P_p - P_{th})}{E_p}, \quad 2.7$$

where  $\eta_s$  is the slope efficiency,  $P_p$  is the pump power and  $P_{th}$  is the threshold pump power threshold.

The intracavity power of a Q-switch microchip configuration with an ideal  $sech^2$  function provides a symmetric Gaussian peak in the regime of interest ( $l \gg q_0$ ), where  $l$  is the sum of losses in the output coupler plus the parasitic losses in the absorber and  $q_0$  is the unbleached values for the absorber. The pulse duration can be estimated at Full Width at Half Maximum (FWHM) by:

$$t_p \approx \frac{3.52 \cdot T_r}{\Delta R} = \frac{7.04 \cdot n \cdot L}{c \cdot \Delta R}, \quad 2.8$$

where  $n$  is the refractive index of the active material,  $L$  is the cavity length and  $c$  is the speed of light in vacuum. The pulse duration is directly proportional to the cavity length, which makes the microchip laser concept very attractive for providing very short laser pulses [29, 48, 50].

## 2. 6. Passive Saturable Absorbers

An SA is an optical element whose transmission changes with intensity. The material becomes more transparent as the intensity increases, and at high intensity values the losses "saturate" and the material is said to "bleach" [135]. The bleaching process is due to the saturation of a quantum transition, which depends on the material.

The most important properties of SAs are the modulation depth, the non-saturable losses, the damage threshold, the recovery time and the saturation fluency (intensity). The modulation depth is the maximum possible change in optical loss where a higher modulation depth increases the peak energy. The non-saturable losses are the parasitic losses that cannot be saturated and which, ideally, must be zero. The damage threshold is the limit at which the material can operate to save its properties. The recovery is the time it takes for the excitation to decay after an excitation pulse. This determines how fast the SA is and should not be too long. Saturation intensity is the intensity required to reduce the absorption to half of its unbleached value and it should be low.

**Table 5.** Properties of some saturable absorbers studied in this thesis

		SWCNTs (2 $\mu\text{m}$ )	1L-G (2 $\mu\text{m}$ )	3L-G (2 $\mu\text{m}$ )	4L-G (2 $\mu\text{m}$ )	MoS <sub>2</sub> (2 $\mu\text{m}$ )	SESA (2 $\mu\text{m}$ )
Saturation Intensity	MW/cm <sup>2</sup>	7	0.6	0.8	1	0.5	23
Modulation Depth	%	0.52	0.23	0.29	0.32	0.32	0.55
Refractive index (SiO <sub>2</sub> )	n <sub>0</sub>	1.43	1.43	1.43	1.43	1.43	/
		Cr <sup>4+</sup> :YAG (1 $\mu\text{m}$ )	V <sup>3+</sup> :YAG (1 $\mu\text{m}$ )	Cr <sup>2+</sup> :ZnS (2 $\mu\text{m}$ )	Cr <sup>2+</sup> :ZnSe (2 $\mu\text{m}$ )		
Ground state absorption cross section	$\sigma_{\text{gsa}}$ (x 10 <sup>-18</sup> cm <sup>2</sup> )	4.5	7.27	0.67	1.3		
Excited state absorption cross section	$\sigma_{\text{esa}}$ (x 10 <sup>-18</sup> cm <sup>2</sup> )	1	7	~0	0.02		
Saturation fluency	J·cm <sup>-2</sup>	0.04	0.03	0.15	0.08		
Recovery time	ns	4000	12	5000	8000		
Refractive index	n <sub>0</sub>	1.82	1.82	2.27	2.45		

In this thesis, SAs consisting of carbon nanostructures (graphene and carbon nanotubes) are studied as well as semiconductor materials (SESAM, MoS<sub>2</sub> and PbS QD in a glass)

and dielectric materials doped with chromium (Cr:ZnS and Cr:YAG). Table 5 shows some properties of the SAs studied.

Carbon nanotubes can be used as SAs because it is a nanostructured material with unique electric and optical properties and a zero band-gap. In particular, single-walled carbon nanotubes, SWCNTs, can be used as saturable absorbers. They have a very broad saturable absorption band. Their properties are mainly determined by the roll direction of the graphene sheet, and they have fast recovery times, relatively low saturation intensities and high damage thresholds [40, 43, 46].

Graphene is another carbon structure whose properties are similar to those of SWCNTs. The flat honeycomb can be used in single or multiple layers of graphene in the broadband of the spectrum. Graphene is a  $sp^2$  hybridisation and has an atomic thickness of  $\sim 0.4\text{nm}$ , which corresponds to the universal transmission of a single-layer graphene,  $T \approx 97.7\%$ . Multiple graphene layers decrease transmission and produce higher modulation depth, which gives high energy pulses [40-42, 44, 47].

2D  $\text{MoS}_2$  structures exhibit broadband absorption saturation in a broad spectral range extending from the visible to  $\sim 2.1\ \mu\text{m}$ . Their saturation fluency is relatively low, the recovery time of the initial absorption is ultrafast, and the mechanical properties are good. This effect is related to the finite density of states in the conduction band in accordance with the Pauli blocking principle, so that at a certain intensity of the incident light, the excitation of carriers from the valence band to the conduction band is blocked and bleaching occurs [136, 137].

The most common dielectric material in passive Q-switching is  $\text{Cr}^{4+}:\text{YAG}$  [38, 138]. This crystal can be used at  $\sim 1\ \mu\text{m}$  as a saturable absorber. Another possibility is  $\text{V}^{3+}:\text{YAG}$  [139], which can also be used at  $\sim 1$  and  $\sim 1.3\ \mu\text{m}$ . Both crystals have slow saturation that can be used in passive Q-switching (up to several ps of pulse duration). These doped:YAG crystals have a transparent window from UV to NIR emission, a high absorption cross section, and thermal, chemical and mechanical properties that are suitable for laser applications.

Another configuration of crystals doped with chromium is the oxidation state of two cations,  $\text{Cr}^{2+}$ . The most common hosts are ZnS and ZnSe [39, 140]. Doped chromium zinc chalcogenides have a broadband absorption between  $1.5$  and  $2.1\ \mu\text{m}$ . The low absorption at

around 2  $\mu\text{m}$ , the fast decay time of the electrons in the excited level and the good mechanical, thermal and optical properties make it possible to use this active material as a saturable absorber. However, these crystals are typically designed for laser emission between 1.8 and 3.5  $\mu\text{m}$ .

Other semiconductor materials for SAs are SESAM and SESA. The difference between them is how they are used – in the transmittance or reflectance mode – or what material the SA is made of. This kind of material has also become a key component for fast lasers. It was not until the 1990s, when theoretical predictions and experimental results indicated the presence of pulse emission. The SESAM is designed as a Fabry-Perot structure with dielectric Bragg mirrors that can be adjusted to reduce the saturation fluency and the losses in the laser cavity, and so determine the modulation depth of the SA device [141-142].

3.

# Objectives

The general objective of this study is to develop compact, efficient and robust SSLs in the near-infrared using different ion-host combinations. This kind of laser can be implemented in numerous applications so that they can be used by people without technical experience and do not need to be aligned.

This study focuses on microchip lasers at several laser wavelengths, particularly at 1 and 2  $\mu\text{m}$ . The general objective outlined above can be subdivided into three specific objectives:

- ✓ The study of TL effects in active materials.
- ✓ CW laser generation in several active materials using the microchip configuration.
- ✓ The study of PQS microchip lasers by novel SAs.

To accomplish the first objective the active materials were studied using diode pumping in a plan-concave linear cavity. The study largely focused on MDT crystals, essentially KLuW doped with Yb, Tm and Ho ions. Borates and garnets (doped with  $\text{Yb}^{3+}$ ) and fluorides and sesquioxides (doped with  $\text{Tm}^{3+}$ ) were also studied.

Once the sign of the TL in these materials had been determined, the second objective was to demonstrate CW laser operation by applying the microchip concept. To this end, a large number of materials were studied: MDTs (doped with  $\text{Yb}^{3+}$ ,  $\text{Nd}^{3+}$ ,  $\text{Tm}^{3+}$  and  $\text{Ho}^{3+}$ ), garnets (doped with  $\text{Yb}^{3+}$  and  $\text{Ho}^{3+}$ ), vanadates (doped with  $\text{Yb}^{3+}$  and  $\text{Tm}^{3+}$ ), borates (doped with  $\text{Yb}^{3+}$ ), fluorides (doped with  $\text{Tm}^{3+}$ ) and sesquioxides (doped with  $\text{Tm}^{3+}$ ). In all cases, the study was performed by pumping with LD, with the exception of  $\text{Ho}^{3+}$ ; Ho:YAG was pumped by a Tm-fibre laser and the Ho-doped MDTs were pumped by a home-made Tm SSL.

The PQS laser performance of the microchip lasers was studied with standard and novel absorbers. Graphene, Single-Walled Carbon Nanotubes (SWCNTs),  $\text{MoS}_2$ , Cr:YAG and V:YAG were studied at 1  $\mu\text{m}$  and graphene, SWCNTs,  $\text{MoS}_2$ , Cr:ZnS, PbS quantum dots and SESAM were studied at 2  $\mu\text{m}$ .

To fulfil these objectives, research groups from all over the world have provided the necessary active materials: SAs, pump sources, suitable mirrors, crystals holders, etc.

# 4.

## Results

4. 1. Continuous-wave laser operation.....	22
4. 2. Thermal lens .....	28
4. 3. Passively Q-switched laser operation .....	31

This section is divided into three parts, one for each of the specific objectives. The most important results are summarized in tables and each topic is discussed in greater depth in the reported papers. The results were grouped according to the active ions of Yb, Nd, Tm and Ho. Most of the results have already been published, but the work is ongoing and more results are expected to be published in short.

## 4. 1. Continuous-wave laser operation

The Yb ions were studied as a dopant in several crystalline hosts. The hosts studied were isotropic gallium garnets ( $\text{Lu}_3\text{Ga}_5\text{O}_{12}$  (LuGG),  $\text{Y}_3\text{Ga}_5\text{O}_{12}$  (YGG),  $\text{Ca}_3(\text{Nb}_{1.5}\text{Ga}_{0.5})\text{Ga}_3\text{O}_{12}$  (CNGG),  $\text{Ca}_3\text{Li}_{0.275}\text{Nb}_{1.775}\text{Ga}_{2.95}\text{O}_{12}$  (CLNGG),  $\text{Y}_3\text{Al}_5\text{O}_{12}$  (YAG), tetragonal aluminates ( $\text{CaGdAlO}_4$  (CALGO) and  $\text{CaYAlO}_4$  (CALYO)), the anisotropic trigonal ( $\text{YAl}_3(\text{BO}_3)_4$  or YAB) and monoclinic ( $\text{Ca}_4\text{Y}(\text{BO}_3)_3$  or YCOB) borates, and the MDTs ( $\text{KLu}(\text{WO}_4)_2$  (KLuW) and  $\text{KLuIn}(\text{WO}_4)_2$  (KLuInW)) (see Table 6).

**Table 6.** The most important CW results with  $\text{Yb}^{3+}$

$\text{Yb}^{3+}$	Pump source	Cut	Doping (at.%)	Thickness (mm)	Polariz.	Max. Abs. (%)	Slope (%)	Max. Pow. (W)	Laser Emission (nm)	Ref.			
KLuW	Ti:Sap.	Ng	25	0.9	E//Nm	54	91	0.308	1059 - 1061	P26, C23			
			5	2.6		57	83	0.201	1043 - 1046				
	LD975		3	3		50	40	0.992	1051	P3			
			3	2.6		44	65	4.4	1049	P6, C10			
	LD981		1.5	2.6		62	78	8.7	1025	In preparation			
			3	2.6		66	86	10.4	1050				
			3	3.3		80	42	4.8	1032				
			5	2.6		72	83	9.4	1042				
	KLuInW		LD975			3.5	3	E//Nm	52	78	4.11	1042 - 1048	P25, C31
	YAB		LD975	c		5	3	E//a	70	67	7.18	1041 - 1044	C29
CALGO	LD975	$\sigma$	8	6	E// $\sigma$	70	84	7.79	1057 - 1065	C25, C30			
	LD981					83	63	9.8	1043 - 1059	In preparation			
CALYO	LD975		3	3	E// $\sigma$	55	91	5.06	1048 - 1056	C25, C30			
	LD981					62	67	5.91	1041 - 1055	In preparation			
LuGG	LD932		/	7.5	6	Unpol.	73	75	8.97	1040	P14, C16		
	LD969				76		65	9.31					
YGG	LD932	6.02		75	61		8.4	1042					
	LD969	65		71	8.68								
CNGG	LD932	5.8		8	71		37	5.05	1051				
	LD969						57	42		4.25			
CLNGG	LD932	5		3.14	47		54	6.18	1039				
	LD969				42		64	6.18					
YAG	LD932	3		3	42		58	0.9	1032	P11, C6			
	LD969				55		36	0.6					

YCOB	LD975	X	3	15	E//Z	50	68	4.16	1043 - 1058	P18, C19
		Y				70	78	4.94	1038 - 1050	
		Z			E//X	60	79	4.65	1035 - 1039	
							70	8.35		

The Yb - doped crystals studied emit light in the 1 - 1.1  $\mu\text{m}$  range. The emission corresponds to the  ${}^2F_{5/2} \rightarrow {}^2F_{7/2}$  transition. The crystals that provide the highest output power in the microchip geometry are the ones with a high degree of symmetry in the crystallographic structure: the garnets. The high thermal conductivity of these crystals provides high output powers and high slope efficiencies. Similarly, the borates show very good laser performance. A systematic study was made of MDTs in an attempt to improve and optimize the output characteristics for power scaling. The study optimized the setup for different doping levels, pump sources, crystal thicknesses, etc. achieving output powers as high as 10 W and slope efficiencies of 91 %. Tables, figures and the complete discussion of each study are included in the papers.

**Table 7.** The most important CW results achieved with Nd. \*Double peak laser oscillator

Nd <sup>3+</sup>	Pump source	Cut	Doping (at.%)	Thickness (mm)	Polariz.	Max. abs (%)	Slope (%)	Max. Pow. (W)	Laser Emission (nm)	Ref.
KGW	LD805	Ng	3	3	E//Nm	54	61	4.02	1067	P21
			10	0.8		72	71	1.05		
	Ti:Sap.		3	0.25		68	74	0.341		
	LD805		42	33		0.906				
	Ti:Sap.	10	0.9	39	74	0.340		P26, C23		
SYSO			0.8	3.02		24	50	1.03	1079	
							16	0.26	1350 - 1390*	
CALGO	LD805	$\sigma$	1	6.37	E//a	74	25	1.75	1081	In preparation
							5	0.16	1350 - 1390*	
CALYO			0.8	5.05		65	35	4.01	1082	
							8	0.37	1350 - 1390*	

The Nd ions were studied as a dopant in  $\text{KGd}(\text{WO}_4)_2$  (KGW), silicate  $\text{Sc}_{0.2}\text{Y}_{0.8}\text{SiO}_5$  (SYSO), and the tetragonal aluminates CALGO and CALYO (see table 7).

The closer atomic radius of Gd and Nd makes KGW the most suitable of the MDTs. It was studied in various scenarios (Table 7) and the maximum slope efficiency was limited by the quantum defect. With highly doped crystals, slope efficiencies were high while power scaling was demonstrated at lower doping levels. Future work will focus on optimizing the doping level/thickness ratio.

**Table 8.** The most important CW results achieved using  $Tm^{3+}$

$Tm^{3+}$	Pump source	Cut	Doping (at.%)	Thickness (mm)	Polariz.	Max. Abs. (%)	Slope (%)	Max. Pow. (W)	Laser Emission (nm)	Ref.	
KLuW	LD805	Ng	3	2.5	E//Nm	62	44	0.88	1950	P1, C1	
						62	50.4	3.2	1946	P2, C2, C10	
	15	2.5	83	77		0.785	1957 - 1965				
	Ti:Sap.	Ng	5	4		42	73	0.525	1950 - 1961	P26, C23	
8			2.9	51	74	0.504	1949				
Lu <sub>2</sub> O <sub>3</sub>	LD805	/	1.8	3	Unpol.	32	50	3.3	2064	P30, C26	
			4	1.7		28	33	2.15	2068 - 2075		
Y <sub>2</sub> O <sub>3</sub>			2.5	2.3		30	27	2.04	2049 - 2065		
Sc <sub>2</sub> O <sub>3</sub>			2	2.2		20	30	1.14	1991 - 2002		
LuVO <sub>4</sub>	LD802	σ	4	3	E//σ	75	39	1.9	1930 - 1960	In preparation	
Na <sub>2</sub> La <sub>4</sub> (WO <sub>4</sub> ) <sub>7</sub>	LD805		E//π		18	31	0.65	1937	C32		
MgWO <sub>4</sub>	LD802	Z	0.9	3.05	E//Y	30	39	0.775	2017 - 2034	P29, C33	
	LD805						50	3.09	2022 - 2034	P33	
		X	1.86	14		50	0.805	2020 - 2057			
GYF	LD792	σ	8	2.7	E//σ	27	65	1.87	1902 - 2005	P32, C28	
YLF				3.38			38	72	3.1		1903 - 2018
LLF				2.63			26	38	1.3		1925 - 2012
				12			3.54	37	52		2.65
KYF	LD802	σ	8	2.8	E//σ	22	79	1.280	1850	In preparation	
CALGO			3	3		30	37	0.695	1950		

In the case of the silicate and aluminate crystals, a longer laser wavelength might make these lasers more attractive for specific applications. The laser wavelength was observed at  $\sim 1.08 \mu m$ . Moreover, we demonstrated laser emission for the  $^4F_{3/2} \rightarrow ^4I_{13/2}$  transition (emission from 1.3 to 1.4  $\mu m$ ). Dual laser wavelength at 1.35 and 1.39  $\mu m$  was observed for the three crystals with relatively low slope efficiencies. The laser emission may oscillate at these two

wavelengths depending on the gain cross-section spectra. Tables, figures and the complete discussion of each study are included in the papers.

The Tm ions were also studied in several host materials: the MDT KLuW, the tetragonal tungstates ( $\text{Na}_2\text{La}_4(\text{WO}_4)_7$  and  $\text{MgWO}_4$ ), the isotropic cubic sesquioxides ( $\text{Lu}_2\text{O}_3$ ,  $\text{Y}_2\text{O}_3$  and  $\text{Sc}_2\text{O}_3$ ), the tetragonal fluorides ( $\text{LiLuF}_4$  (LLF),  $\text{LiYF}_4$  (YLF),  $\text{LiGdF}_4$  (GYF) and  $\text{YKF}_4$  (KYF)) and the tetragonal aluminate (CALGO) and vanadate ( $\text{LuVO}_4$ ) (see table 8). Moreover a co-doped MDT Yb,Tm:KLuW laser has been reported at 2  $\mu\text{m}$  (table 9).

The transition in Tm that corresponds to a  $\sim 2 \mu\text{m}$  emission is the  $^3\text{F}_4 \rightarrow ^3\text{H}_6$ . This transition, after pumping at around 800 nm, leads to the so-called cross-relaxation mechanism [18] that significantly reduces the quantum defect, which gives two photons instead of only one pump photon.

**Table 9.** The most important CW results achieved using co-doped  $\text{Yb}^{3+}$ - $\text{Tm}^{3+}$  crystals

$\text{Yb}^{3+}$ , $\text{Tm}^{3+}$	Pump source	Cut	Doping (%)	Thickness (mm)	Polariz.	Max. Abs. (%)	Slope (%)	Max. Pow. (W)	Laser Emission (nm)	Ref.
KLuW	Ti:Sap.	Ng	5 - 6	3	E//Nm	86	27	0.082	1995 - 2010	P26, C23
			5 - 8			74	20	0.201	1990 - 2007	
	5 - 6		14			0.142	1994 - 2010	P13, C8		
	LD975		2.5 - 8			15	0.156		1990 - 2005	
	2.5 - 4		50			15	0.198		1995 - 2010	
	2.5 - 2.5		10			0.125	1975 - 1992			

KLuW was systematically studied with two different pump sources, and several doping levels and thicknesses. Power scaling was demonstrated and a record slope efficiency of 77% was achieved with Ti:Sapphire laser pumping. Highly doped Tm MDTs are good candidates for highly efficient, compact lasers (very short gain medium). In general, the rest of the materials studied show very promising results. By optimizing many of them, output powers and slope efficiencies can be very high (for example, Tm:MgWO<sub>4</sub>). However, those with relatively low thermal conductivity are limited to power scaling: i.e. Na<sub>2</sub>La<sub>4</sub>(WO<sub>4</sub>)<sub>7</sub> with only 31 % and 0.65 W. Tables, figures and the complete discussion of each study are included in the papers.

The co-doped single crystal with Yb as a sensitizer of the Tm emission was studied as an alternative to the pump scheme studied before [143]. The optimal doping ratio was determined (Table 9). However, the limited energy transfer from Yb to Tm affects the thermal component of the laser system. Due to the pump scheme (pumping at 981 nm), the up-conversion losses became stronger, leading to an increase in the heat in the crystal, which meant that the laser performance was not as good as that of the singly-doped one. The optimum doping ration was 5 at.% Tm<sup>3+</sup> and 8 at.% Yb<sup>3+</sup> at which the output power and slope efficiency were maximum. Using a Ti:Sapphire laser as pump source with excellent mode matching and a polarization parallel to the  $N_m$  principal optical direction helped to make the slope of the laser more efficient. A complete study with different cavity schemes and transmission of the output couplers can be found in the published papers.

As for the Ho ion, the MDTs (KLuW and KYW) and a cubic ceramic based on YAG have been studied (see table 10). The Ho ions were also studied in a co-doped system with Tm ions in a MDT (KluW) and the tetragonal fluoride (YLF) (see Table 11).

**Table 10.** The most important CW results achieved using Ho<sup>3+</sup>

Ho <sup>3+</sup>	Pump source	Cut	Doping (%)	Thickness (mm)	Polariz.	Max. Abs. (%)	Slope (%)	Max. Pow. (W)	Laser Emission (nm)	Ref.
KLuW	Tm:KLuW	Ng	3	2.67	E//Nm	25.5	84	0.201	2105	<b>P5, C10</b>
	Intrac.					88	0.53	2080	<b>P10</b>	
	3at%Tm:KLuW					-	8.3	0.29	2080	<b>P7, C11</b>
KYW	Tm:KLuW			2.7		26	85	0.205	2105	<b>P22, P26, C23</b>
YAG - ceramic	Tm-Fibre	/	1	4	Unpol.	33	88	1.18	2090	<b>P31</b>

The main problem for singly doped Ho crystals is to find suitable pump sources since they have to be resonantly pumped at  $\sim 1.9 \mu\text{m}$ . GaSb-based diodes are rather expensive and not flexible in the emission wavelength. The alternative to the laser diodes are fibers and SSLs that can be tuned to match Ho's absorption maximum. However, generally speaking, fiber lasers are also relatively expensive while tuned SSL do not have enough pump power. The

available Tm-fiber in this study emitted at 1910 nm, which coincided with the absorption band of Ho:YAG ceramic.

**Table 11.** The most important CW results achieved using co-doped Tm<sup>3+</sup>- Ho<sup>3+</sup> crystals

Tm <sup>3+</sup> , Ho <sup>3+</sup>	Pump source	Cut	Doping (%)	Thickness (mm)	Polariz.	Max. Abs. (%)	Slope (%)	Max. Pow. (W)	Laser Emission (nm)	Ref.
KLuW	LD805	Ng	5 - 0.5	2.86	E//Nm	60	31	0.45	2081	P4
				1.5		47	17	0.4	2081	
	Ti:Sap.	7 - 0.25	3	52	58	0.32	2061	P26, C23		
YLF	LD802	σ	5 - 0.5	3.68	E//σ	40	25	0.378	2065	P32

A ~3 W home-made Tm:KLuW laser was developed to pump Ho-doped KLuW. The excellent beam quality and mode-matching gave a slope efficiency of 88 % with the Ho laser. For the intracavity pumping geometry (Table 10) the performance was inferior, largely because of the non-optimized doping level, the thicknesses of the crystals and, particularly the fact that the crystals were uncoated so the intracavity losses were very high. A complete study with different cavity schemes and transmission of the output couplers can be found in the papers.

To find a more conventional pump source, co-doping with Tm was studied. However, as with Yb-Tm, the energy transfer between ions limits the maximum slope efficiency and output power reached and there are important up-conversion losses. The optimum co-doping ratio is 1:10 for Ho and Tm, respectively (see Table 11). Concentrations higher than 0.5 at.% for Ho substantially mitigate the laser performance and clearly damage the samples when pump powers were high. A complete study with different cavity schemes, and transmission of the output couplers can be found in the published papers.

## 4. 2. Thermal lens

A comparative study of TL for Yb-doped MDTs and oxoborates, both being of which are biaxial crystals, was performed along the three principal axes. The results are reported for cubic garnet. Table 12 shows the main thermo- optic parameters for the study of the thermal lens. The complete study and all data can be found in the published papers.

**Table 12.** The most important TL results achieved for Yb<sup>3+</sup>

Yb <sup>3+</sup>	Cut	Polariz.	Plane	M-factor, (m <sup>-1</sup> /W)	S degree, m <sup>-1</sup> /W	S/M <sub>MAX</sub> (%)	dn/dT 10 <sup>-6</sup> K <sup>-1</sup>	P <sub>pe</sub> 10 <sup>-6</sup> K <sup>-1</sup>	Q <sub>distr</sub> 10 <sup>-6</sup> K <sup>-1</sup>	X 10 <sup>-6</sup> K <sup>-1</sup>	Ref.
KLuW	Ng	E//Nm	pg - plane	+2.8	0.7	20%	-6.5	+0.4	+13.3	+7	P3
			mg - plane	+3.5				+2.2		+9	
	Nm	E//Np	pm - plane	-2	2.4	120%	-14.6	-2.4	+11	-6	
			gm - plane	+0.4				+4.8		+1.2	
	Np	E//Nm	gp - plane	-1.6	2.5	156%	-6.5	-1.1	+3.4	-4.2	
			mp - plane	+0.9				+5.4		+2.3	
YCOB	X	E//Z	ZX - plane	+4.1	0.3	7%	-2.5	-1.2	+10.6	+6.9	P18, C19
			YX - plane	+3.8				-1.7		+6.4	
	Y	E//Z	XY - plane	+1	0.9	47%	-2.5	+1.9	+2.3	+1.7	
			ZY - plane	+1.9				+3.4		+3.2	
	Z	E//X	YZ - plane	+2.8	0.4	14%	-1.2	+1.9	+4.9	+5.6	
			XZ - plane	+2.4				+1.1		+4.8	
CNGG				+5			+8.8	+0.6	+5.4	14.8	
CNLGG				+3.9			+8.4	+0.7	+5.3	14.4	P14
YGG	/	Unpol.	/	+2	/	/	+8.4	+0.6	+4.3	13.3	
LuGG				+2.1			+8.1	+0.6	+5.2	13.9	

For MDTs the thermal lens is positive only along the N<sub>g</sub> principal direction, for oxoborate YCOB it is positive along all propagation directions, X, Y and Z, and for all the garnets studied it is positive. The positive thermal lens makes it possible to produce microchip lasers independent of the laser wavelength. This configuration provides a TEM<sub>00</sub> laser mode and the degree of circular beam is given by the sensitivity factor of the thermal lens, the M- factor. This number can be evaluated by the degree of astigmatism, defined as S. As for the isotropic

garnets with positive TL, the best crystal to operate in the microchip configuration is YGG because it gives the lowest  $S$  and circular beam at different absorption levels. To study the planes of light propagation in uniaxial and biaxial crystals, the circularity of the laser beam, which depends on the sensitivity factor, needs to be evaluated. All planes of propagation in the monoclinic oxoborate have positive TL with the lowest values of  $M$  along the  $Y$  direction. However, this cut has stronger astigmatism than the other two cuts, and at high absorbed power the circular beam turns elliptical.

**Table 13.** The most important TL results achieved using  $Tm^{3+}$  and  $Tm^{3+}, Ho^{3+}$

$Tm^{3+}$	Cut	Polariz.	Plane	$M$ -factor, $m^{-1}/W$	$S$ degree, $m^{-1}/W$	$S/M_{MAX}$ (%)	$dn/dt$ $10^{-6}K^{-1}$	$P_{pe}$ $10^{-6}K^{-1}$	$Q_{distr}$ $10^{-6}K^{-1}$	$X$ $10^{-6}K^{-1}$	Ref.
<b>KLuW</b>	$N_g$	$E//m$	$pg$ -plane	+12.9	4.8	37	-5.9	+1.7	+13	+8.8	<b>P1, P2, C1,</b>
			$mg$ -plane	+8.1				-1.6		+5.5	
	$N_m$	$E//p$	$pm$ -plane	+1.5	8.1	122	-12.3	+3	+10.8	+1.5	
			$gm$ -plane	-6.6				-0.5		-2	
	$N_p$	$E//m$	$gp$ -plane	+3.4	9.5	155	-5.9	+3.3	+3.3	+0.7	
			$mp$ -plane	-6.1				-1.3		-3.9	
<b>YLF</b>			$\pi$ $\sigma$ -plane	+4	0.4	10	-5.6	-2.1	+12.1	+4.4	<b>P32, C28</b>
			$\sigma$ $\sigma$ -plane	+3.6				-2.5		+4.0	
<b>GLF</b>	$\sigma$	$E//\sigma$	$\pi$ $\sigma$ -plane	+5.6	1.4	25	-6	-1.8	+17.2	+9.4	
			$\sigma$ $\sigma$ -plane	+4.2				-1.6		+9.6	
<b>LLF</b>			$\pi$ $\sigma$ -plane	+4.3	0.4	9.3	-3.6	-2	+12.2	+6.6	
			$\sigma$ $\sigma$ -plane	+3.9				-3.3		+5.3	
<b>Lu<sub>2</sub>O<sub>3</sub></b>				+3.7			+9	+2.3	+7.6	+18.9	
<b>Y<sub>2</sub>O<sub>3</sub></b>	/	Unpol	/	+6.9	/	/	+7.9	0.7	+7.9	+16.5	<b>P30</b>
<b>Sc<sub>2</sub>O<sub>3</sub></b>				+8.3			+8.4	+1.9	+8.5	+18.8	
$Tm^{3+}, Ho^{3+}$	Cut	Polariz.	Plane	$M$ -factor, $m^{-1}/W$	$S$ degree, $m^{-1}/W$	$S/M_{MAX}$ (%)	$dn/dt$ $10^{-6}K^{-1}$	$P_{pe}$ $10^{-6}K^{-1}$	$Q_{distr}$ $10^{-6}K^{-1}$	$X$ $10^{-6}K^{-1}$	Ref.
<b>KLuW</b>	$N_g$	$E//m$	$pg$ -plane	+24.1	0.8	4	-6	+2.1	+13	+9.1	<b>P4</b>
			$mg$ -plane	+24.9				+2.4		+9.4	

Table 13 shows the study of the TL for Tm-doped MDTs, cubic sesquioxides,  $X_2O_3$  (where  $X = Lu, Y$  and  $Sc$ ) and the tetragonal  $LiXF_4$  fluorides (where  $X = Y, Gd$  and  $Lu$ ) along the  $a$  propagation direction. As for Tm and Ho in MDTs, there are no significant differences in  $S$  and

$M$  compared to the Yb counterparts. We can conclude that they will behave similarly at low-medium absorbed powers. Also, data for the co-doped Tm, Ho:MDTs are reported. The complete study and all data can be found in the published papers.

The isotropic sesquioxide crystals have positive TL. In this regard, the best crystal to operate in the microchip configuration is  $\text{Lu}_2\text{O}_3$  because it gives the lowest  $S$  and circular beam at low-medium absorbed powers. The worst crystal of this family is  $\text{Sc}_2\text{O}_3$  with a  $M$  of  $+8.3 \text{ m}^{-1}/\text{W}$ . Along the  $a$  direction,  $a$ -cut, the tetragonal fluorides also have positive TL with the YLF crystal having the lowest value of  $M$ . The value of  $S$  between the two planes is lower than for GLF but similar to LLF. The  $M$  value of the YLF crystal is closer to zero.

The TL in co-doped Tm, Ho:KLuW along the  $N_g$  principal optical direction has also been studied (see Table 13). It has a strong  $M$  factor of  $+24.9 \text{ m}^{-1}/\text{W}$  but low  $S$ . The latter guarantees an almost circular laser mode, but the strong deformation of the crystal faces does not allow for power scaling.

### 4. 3. Passively Q-switched laser operation

Yb, Tm and Ho were studied in the microchip configuration by inserting the SA between the gain material and the output coupler to reduce the internal losses and the length of the cavity. Tables, figures and the complete discussion of each study are included in the papers referenced.

The Yb lasers were studied in the passively Q-switched regime for different hosts (see Table 14). Novel nanomaterials, such as single-layer graphene, three-layer graphene, MoS<sub>2</sub> and SWCNTs were studied. The main conclusion for these novel SAs, however, is that further improvement is needed if their modulation depth is to be controlled and, hence, the laser results improved. The exception to this are the SWCNTs that have a rather mature technology. Moreover, more standard materials like Cr<sup>4+</sup>:YAG were tested.

**Table 14.** The most important Q-switched laser results achieved with Yb<sup>3+</sup>

Yb <sup>3+</sup>	SA	Slope (%)	Max. Average Power (W)	Laser Emission (nm)	Peak Energy (μJ)	Peak Power (W)	Polariz.	FWHM (ns)	PRF (kHz)	Ref.
KLuW	1L-Graph.	6	0.113	1030	0.47	1.7	E//Nm	280	240	P17
		12	0.170	1030	0.49	3		165	350	C13
	3L-Graph.	12	0.315	1032	1	7		140	320	P23
	MoS <sub>2</sub>	7	0.147	1030	0.5	2.2		220	300	P23, C21
	Cr:YAG	55	0.59	1031	47.6	7000		0.69	12.4	P20, C24
41		1.51	1038	58	7300	8	26	C9		
YAB	Cr:YAG	53	2.82	1042	47	6600	E//a	7.1	60	C29
CALGO	SWCNTs	14	0.436	1057-65	1.94	7.54		257	225	In preparation
LuGG	1L-Graph.	15	0.32	1041	1.3	2.7	Unpol.	490	245	P16, C15
YGG		23	0.462	1039	1.8	4.1		440	260	
CNGG		24	0.44	1045	1.9	10		190	235	
YAG		12	0.185	1032	0.65	2.9		228	285	P11, C6
		9	0.083		0.41	1.3		323	202	
LuVO <sub>4</sub>		17	0.31	1021	0.94	3.9	E//c	240	330	P17

The maximum average output power, higher  $\eta$ , shortest pulse durations, etc. were clearly given by the standard Cr<sup>4+</sup>:YAG SA. The processing was high quality and the modulation depth was precisely controlled. As mentioned above, the fabrication of the novel SAs needs to be further improved.

As for Q-Switched Tm lasers, several hosts have been studied with the above-mentioned novel SAs as well as more standard polycrystalline Cr:ZnS. In addition, a SESA was also applied only for one crystal for purposes of comparison ( Table 15).

**Table 15.** The most important Q-switched laser results achieved using Tm<sup>3+</sup>

Tm <sup>3+</sup>	SA	Slope (%)	Max. Average Power (W)	Laser Emission (nm)	Peak Energy ( $\mu$ J)	Peak Power (W)	Polariz.	FWHM (ns)	PRF (kHz)	Ref.
KLuW	1L-Graph.	13	0.31	1948	1.6	6	E//Nm	285	190	P8, P27, C5
		11	0.04	1921 - 1944	1	0.3		3700	39	P9, C3
	3L-Graph.	39	1.03	1926	4	20.9		190	260	P23, P27
	SWCNTs	29	0.7	2131	1.1	44		25	620	P24, C20
		12	0.26	1913	0.51	5.3		97	350	P28, C14, C17
	Cr:ZnS	21	0.146	1847	25.6	3280		0.78	5.6	P12, C18
MoS <sub>2</sub>	43	1.27	1929	7.5	42.7	175	170	P23, C21		
LuVO <sub>4</sub>	SESA	12	0.27		0.77	16		46	350	
	SWCNTs	13	0.312	1869 - 1882	1.88	55	E//a	34	166	In preparation
	4L-Graph.	15	0.363		0.72	8.5		86	498	
MgWO <sub>4</sub>	Cr:ZnS	23	0.872	2017	16.1	1184		13.6	54.2	
	SWCNTs	22	0.317	2006 - 2021	1.5	12.6	E//Y	117	215	P33
	1L-Graph.	18	0.274	2012 - 2015	1.2	6		201	229	
LLF	MoS <sub>2</sub>	42	1.130	1920	4.6	31	E//a	147	248	In preparation

Particular effort was made to study graphene as an SA. Commercial graphene as well as home- made graphene with single and several carbon layers were studied and compared. This was especially true of Tm:KLuW, whose three carbon layers were considered to be optimum because of the compromise between modulation depth and scattering losses.

The Ho-based lasers were also Q-switched. These lasers consisted of crystals and ceramics and can be seen in Table 16. Again, novel SAs such as SWCNTs, MoS<sub>2</sub> or SESA were studied for these lasers. In addition, quantum dots (QD) of PbS nanocrystals dispersed in a glass were studied as SAs for these lasers because the absorption band of the QDs lies above 2 μm in the spectral range which makes them highly suitable for Ho Q-switched lasers. Moreover, the co-doped laser system, Tm-Ho was also Q-switched using a single layer graphene and the polycrystalline Cr:ZnS SAs as shown in Table 16.

**Table 16.** The most important Q-switched laser results achieved using Ho<sup>3+</sup>

Ho <sup>3+</sup>	SA	Slope (%)	Max. Average Power (W)	Laser Emission (nm)	Peak Energy (μJ)	Peak Power (W)	Polariz.	FWHM (ns)	PRF (kHz)	Ref.
KLuW	PbS QD glass	42	0.09	2061	1.2	22	E//Nm	30	69	P10, C4, C14
	MoS <sub>2</sub>	48	0.125	2076	0.46	3		150	271	C22
	SWCNTs	21	0.05	2079	0.31	3		100	160	
YAG - ceramic	SESA	37	0.45	2089	3.2	36.9	/	89	141	P31, C27
Tm <sup>3+</sup> , Ho <sup>3+</sup>	SA	Slope (%)	Max. Average Power (W)	Laser Emission (nm)	Peak Energy (μJ)	Peak Power (W)	Polariz.	FWHM (ns)	PRF (kHz)	Ref.
KLuW	1L-graph.	4	0.074	2061	0.2	1	E//Nm	200	340	P15, C7, C14
	Cr:ZnS	11	0.131		9	1150		14	14.5	P19, C12



5.

# Conclusions

In conclusion, this study has shown that the microchip configuration is a good option for efficient laser generation in several active media with positive TL. The thermo-optic behaviour is responsible for stabilizing the mode in this kind of laser resonator and performance is best with crystals with very weak astigmatism of the TL. In these cases a near-circular TEM<sub>00</sub> output beam  $M^2_{x,y} < 1.2$  was achieved in all materials studied. In this study, continuous improvements were made to various aspects of the laser: for example, the crystal holder for optimum cooling, the pump source, non-“standard” output couplers, crystal size and doping, etc. The microchip concept is also a good option for the Q-switched regime, the laser operation of sub-nanosecond pulses has been demonstrated and Q-switched lasers have been produced with novel nanomaterials such as SAs. The main achievements for each active ion studied here are listed below.

### Ytterbium-doped materials

- ✓ The concept of continuous-wave power scaling was demonstrated in Yb:KLuW crystals. Output power was 11 W and slope efficiency 88 %. The TL was studied for light propagation along the three principal optical axes,  $N_p$ ,  $N_m$  and  $N_g$ , of which only  $N_g$  gave a pure positive thermal lens. Passive Q-switching of this Yb laser was demonstrated with graphene, multilayer MoS<sub>2</sub>, V:YAG and Cr:YAG as saturable absorbers. The shortest pulse duration achieved was 690 ps with 47.6  $\mu$ J pulse energy at a pulse repetition frequency of 12.4 kHz. Self-Raman conversion of the fundamental emission to the first Stokes was demonstrated. With suitable mirrors the 120 mW output power achieved might be improved. By pumping with a Ti:Sapphire laser, a highly doped crystal (25 at.% thin sample) reached  $\eta = 91\%$ . Adding indium to the structure did not affect the continuous-wave results in short cavities with conditions similar to Yb:KLuW.
- ✓ The monoclinic *c*-cut Yb:YAB crystal was used in the microchip configuration to achieve 7.18 W in CW at 1041-1044 nm with a slope efficiency of 67 %. Using a Cr:YAG SA, passively Q-switching was achieved with an average output power of 2.02 W with 4.9 ns stable pulse duration corresponding to 83  $\mu$ J pulse energy.
- ✓ The  $\alpha$ -cut Yb:CALGO and Yb:CALYO crystals were shown to be highly-efficient diode-pumped microchip lasers. An 8 at.% doped Yb:CALGO laser generated 7.79 W at 1057-1065 nm with a slope efficiency of 84 %. Power scaling was verified with a 981 nm VBG laser diode and achieved 9.8 W for Yb:CALGO and 5.9 W for a 3 at.% Yb:CALYO crystal limited by the pump power of the diode. Both lasers produced linearly polarized output ( $\sigma$ -polarization).
- ✓ CW microchip laser operation was studied in Yb:LuGG, Yb:YGG, Yb:CNGG, Yb:CNLGG and Yb:YAG under 932 and 969 nm pumping. Laser performance was best for Yb:LuGG, generating 8.97 W of output power with a slope efficiency of 75% and 9.31 W with a slope efficiency of 65%, for the two pump wavelengths, respectively. The TL was studied in all crystals. PQS with graphene as an SA was studied in all crystals. For Yb:CNGG, 190 ns/1.9  $\mu$ J pulses at a repetition frequency of 235 kHz were achieved. Further power scaling seems

feasible by pumping at 969 nm whereas the stronger heat load pumping at 932 nm was a limiting factor.

- ✓ The Yb:LuVO<sub>4</sub> microchip laser was studied in CW and PQS regimes. The use of graphene as an SA generated 152 ns/ 0.83 μJ pulses at 1024 nm with an average output power of 300 mW.
- ✓ The TL was studied in the monoclinic Yb:YCOB with a positive thermal lens in all orientations. The Z-cut crystal has the lowest degree of astigmatism because of the large thermal expansion and strong photo-elastic effect. CW microchip lasers were produced with three cuts while for Z-cut, maximum output power was 8.35 W at ~1040 nm with a slope efficiency of 70%.

#### **Neodymium-doped materials**

- ✓ Monoclinic Nd:KGW cut along the  $N_g$  axis of the optical indicatrix was studied under diode pumping in microchip configuration generating ~4 W of CW at 1067 nm with a slope efficiency of 61 %. Highly-doped 10 at.% Nd:KGW, 250 μm thick crystal had a slope efficiency of 74 % with Ti:Sapphire laser pumping. The slope efficiency reached the theoretical value limited by the quantum defect.
- ✓ The tetragonal Nd:CALGO, Nd:CALYO and Nd:SYSO crystals were also studied by pumping at 805 nm. Output power/efficiency was best with a 0.8 at.% Nd:CALYO laser (365 mW/ 8 % with two laser wavelength oscillating simultaneously at 1350 nm and 1390 nm). All the tetragonal structures produced linearly  $\sigma$  polarized output laser.

#### **Thulium-doped materials**

- ✓ Multi-watt continuous-wave laser operation was demonstrated in Tm:KLuW crystals achieving 3.2 W with a slope efficiency of 50.4 % at 1946 nm. Pumped by a Ti:Sapphire laser, a highly doped crystal (15 at.%) reached a slope efficiency of 77%. The comparative study of the TL demonstrates that only  $N_g$ -cut crystals provide a pure positive thermal lens. PQS was demonstrated with aligned and spaghetti-like Single Walled Carbon Nanotubes, multilayer MoS<sub>2</sub> and Cr:ZnS with a shortest pulse duration of 780 ps/ 25.6 μJ at a pulse

repetition frequency of 5.6 kHz. With a special output coupler (band-pass filter), vibronic laser operation was demonstrated at 2130 nm.

- ✓ The sesquioxides  $\text{Tm:X}_2\text{O}_3$ , where  $X = \text{Lu}, \text{Y}$  and  $\text{Sc}$  were studied to compare their thermo-optic properties and their laser performance in microchip configuration. The TL was positive in all three crystals. The sensitivity factor of the thermal lens was lowest for  $\text{Tm:Lu}_2\text{O}_3$ . This crystal produced 3.3 W output power at 2063 nm with a maximum slope efficiency of 50%. Further power scaling is expected at an optimized Tm doping level.
- ✓ A novel laser crystal,  $\text{Tm:MgWO}_4$ , was reported in CW regime. The first demonstration, using a hemispherical cavity reached a maximum output power of 772 mW with a slope efficiency of 39%. The power-scaled laser using the microchip configuration up to 3.1 W emitted at 2.034  $\mu\text{m}$ .
- ✓ The tetragonal  $\text{Tm:LiLnF}_4$  crystals, where  $\text{Ln} = \text{Y}, \text{Gd}$  and  $\text{Lu}$  were studied to compare their thermo-optic properties and laser characteristics in microchip configuration. For  $a$ -cut crystals the thermal lens was observed to be positive, weak and nearly spherical.  $\text{Tm:YLF}$  has the minimum degree of astigmatism degree and the best laser performance, which generates a maximum output power of  $\sim 3$  W at 1904 nm and a slope efficiency of 72%. Power scaling with the optimization of the Tm doping level is expected. PQS using a multilayer  $\text{MoS}_2$  saturable absorber was studied generating 130 ns/ 4.1  $\mu\text{J}$  pulses at 1920 nm with 1050 mW of average output power.

#### **Ytterbium-thulium co-doped materials**

- ✓ A comprehensive laser characterization of the monoclinic Yb,  $\text{Tm:KLuW}$  crystal was also reported. Using a hemispherical cavity and a 5 at.% Yb – 6 at.% Tm doped crystal, a maximum of 227 mW of CW output power was achieved at 1983-2011 nm. In the case of its performance in microchip configuration, for a 5 at.% Yb – 8 at.% Tm doped crystal a maximum output power of 201 mW at 1990-2007 nm was achieved.

### **Holmium-doped materials**

- ✓ The CW  $N_g$ -cut Ho:KLuW microchip laser in-band-pumped by a Tm:KLuW laser at  $\sim 1.96 \mu\text{m}$  was studied. The experiments achieved a maximum slope efficiency of 88%, delivering 530 mW output power at  $2.08 \mu\text{m}$ . The PQS of this laser was also reported using several SAs, such as graphene, MoS<sub>2</sub>, single walled carbon nanotubes and PbS QDs. The shortest pulses had 30 ns/ 0.5  $\mu\text{J}$  pulse duration and pulse energy, respectively at a pulse repetition frequency of 62 kHz. A compact intracavity-pumped microchip Ho-laser was produced using stacked Tm:KLuW/Ho:KLuW crystals pumped by a laser diode at 805 nm. Dual laser wavelength with a maximum continuous-wave output power of 887 mW (285 mW from Ho) and a slope efficiency of 23 % was achieved operating at 1867-1900 nm (Tm<sup>3+</sup> emission) and at 2078-2100 nm (Ho<sup>3+</sup> emission).
- ✓ Ho:YAG transparent ceramics were also studied in PQS regime with a semiconductor SA. The laser generated a maximum average output power of 610 mW at 2089 nm and a maximum slope efficiency of 51%. Pulses were as short as  $\sim 100 \text{ ns}$ / 2.9  $\mu\text{J}$  at repetition rates of 210 kHz. Increasing the modulation depth of the semiconductor saturable absorber at  $2.1 \mu\text{m}$  makes it possible to scale the pulse energy and reduce the pulse duration.

### **Thulium-holmium co-doped materials:**

- ✓ The TL effect in monoclinic Tm, Ho:KLuW cut for light propagation along the  $N_g$  optical indicatrix axis was measured and was found to be positive in both planes. In microchip configuration, laser with a maximum output power of 450 mW and a slope efficiency of 31% was achieved oscillating in the 2060-2096 nm spectral range. In Q-switched regime with Cr:ZnS as an SA, the average output power was 131 mW at 2063.6 nm. The slope efficiency was 11 % and the conversion efficiency with respect to the continuous-wave regime was 58%. The pulse characteristics were 14 ns / 9  $\mu\text{J}$  at a pulse repetition frequency of 14.5 kHz. The simulations were in good agreement with the experimental results.



6.

# Appendix

This section briefly describes the most important equipment used to obtain the results in this study. Devices such as pump sources, pump and output coupler mirrors, crystal holders, cavity setups, external devices, electrospinning, crystal growth devices, cutting and polishing devices, spectroscopy and microscopy equipment are described.

## 6.1 Pump sources

When working with different active ions, Yb, Nd, Tm and Ho, several pump sources are required if the desired laser is to be achieved. The pump source depends on the absorption band (energy levels of the active ions) and it is affected by the atomic structure of the host. The following pump sources have been used in this study.

### ✓ **Ti:Sapphire laser**

A Mode-locked Coherent MIRA 900 Ti:Sapphire laser was used. It has a tuneable laser emission from 700 to 1000 nm and a maximum power of 2 W at 800 nm. The Ti:Sapphire laser was pumped by a Verdi 532 nm which delivered 10 W with good stability and reliability. For the laser experiments, the Ti:Sapphire laser was adapted for CW operation. This laser provides a good  $M^2 \sim 1$  factor, polarized light and little divergence, which provides excellent mode matching with the laser mode of the microchip resonator. This pump source was used for  $Tm^{3+}$ ,  $Nd^{3+}$  and  $Yb^{3+}$  ions as described in [P26, C23].

### ✓ **Laser Diodes**

A set of commercial fibre-coupled laser diodes operating at  $\sim 791$  nm,  $\sim 802$  nm  $\sim 805$  nm,  $\sim 936$  nm,  $\sim 969$  nm,  $\sim 980$  nm and  $\sim 981$  nm was used to pump the crystals in the CW and Q-switched regimes. All of these laser diodes were used with different fibres to provide unpolarized light.

The 791 nm AlGaAs laser diode had a core diameter of 105  $\mu m$  with a numerical aperture (NA) of 0.15. The laser diode was temperature-tuned at 25°C and emitted at 791 nm with an air-cooling system at a maximum output power of 10W. The wavelength was shifted  $\pm 4$  nm by controlling the peak wavelength and reaching the maximum absorption in the active material with a small bandwidth at the peak of emission. This diode was used for the  $Tm:LiLnF_4$  lasers ( $Ln=Y, Gd, \text{ and } Lu$ ) [P32, C28].

The 802 nm diode is an AlGaAs laser diode with a core diameter of 105  $\mu\text{m}$  controlled by an air-cooling system. The laser diode delivers a maximum output power of 10 W with an NA of 0.15. It was used for Tm:MDTs and vanadates [P24, P35, C20].

The 805 nm laser module had a core diameter of 200  $\mu\text{m}$  with a spectral width of 6 nm. The wavelength could be shifted  $\pm 5$  nm depending of the temperature of the diode. It delivered 30 W with an NA =0.22 and was used to pump the Tm:MDTs and sesquioxides. The diode was also used to excite the Nd:MDT, aluminate and silicate crystals [P1, P2, P4, P5, P7-P10, P12, P15, P19, P21, P22, P27-P30, P37, P39, P40, C1-C5, C7, C10-C12, C14, C17, C18, C21, C22, C26].

The 936 nm, 969 nm and 981 nm diode lasers were operated by a water cooling system. The core diameters were 105  $\mu\text{m}$ , 200  $\mu\text{m}$  and 105  $\mu\text{m}$  with NAs of 0.14, 0.22 and 0.14, respectively. They all had a maximum output power of 27 W. The 936 nm laser had a spectral width of  $\sim 5.5$  nm and a temperature-tuned emission between 928 nm and 939 nm. The 969 nm and 981 nm diodes were stabilized by a Volume Bragg Grating with a FWHM of  $\sim 0.3$  and could be shifted  $\pm 0.1$  nm. The single emitters were controlled by an external power supply. The 932 nm and 969 nm diode lasers were used to pump the garnets [P11, P14, C6, C16] and the 981 nm laser was used to pump the Yb:MDTs and aluminates [P33, P34, P38].

The 980 nm compact laser diode delivered 50 W of output power with a core diameter of the fibre of 200  $\mu\text{m}$  and an NA of 0.22. The influence of the temperature could shift the position of the wavelength emission from 968 to 985 nm with a FWHM of  $\pm 3$  nm. This diode was used to pump the Yb-doped borates, MDTs, garnets, aluminates and vanadates [P3, P6, P13, P16-P18, P20, P23, P25, P31, P38, C8-C10, C13, C15, C19, C21, C24, C29, C30, C31]

### ✓ **Tm Laser**

This TEM<sub>00</sub> mode home-made laser delivered a maximum output power of 3 W with good stability and polarized light. It consisted of a diode-pumped Tm:KLuW laser operating at 1946 nm. The details of the Tm:KLuW laser can be found in [P2]. It was used to pump the Ho:KREW crystals ( $RE = \text{Y, Gd, Lu}$ ) [P5, P7, P10, P22, P29, C4, C10, C14, C22].

✓ **Tm-fibre Laser**

The Tm-fibre laser emitted up to 5 W at 1910 nm with a core diameter of 400  $\mu\text{m}$ . It provided a collimated un-polarized output beam with a spectral linewidth of 0.7 nm. The full divergence angle is 0.58 mrad, which corresponds to a  $M^2 = 1.05$  with very good TEM<sub>00</sub> laser mode. This fibre laser was used for the Ho:YAG ceramics [C27].

## 6.2 Optical elements

The input and output mirrors are crucial for the laser resonator. Table 17 shows the mirrors with specific coatings that were needed to produce the lasers studied in this thesis. Each mirror consists of two different coatings, the internal and the rear faces with respect to the cavity.

**Table 17.** Mirrors used in this study for the CW and Q-switched regimes. <sup>\*1</sup>The rear face is HT from 0.9 to 1.1  $\mu\text{m}$ . <sup>\*2</sup>The rear face is HT from 0.8 - 1.1  $\mu\text{m}$  and 1.3 - 1.5  $\mu\text{m}$ . <sup>\*3</sup>The rear face is HT from 0.8 – 1  $\mu\text{m}$  and HT from 1.8 – 2.075  $\mu\text{m}$ . <sup>\*4</sup>The rear face is HT from 1.9 – 2  $\mu\text{m}$ . PM= Pump Mirror, HR= High Reflector, HT= High Transmission PR= Partial Reflection, OC, output coupler,  $R_{OC}$ = Radius curvature of the concave output couplers

Set of mirrors (internal face)						
	At 1 $\mu\text{m}^{*1}$		At 1.3 $\mu\text{m}^{*2}$		At 2 -2.1 $\mu\text{m}^{*3}$	
	HT ( $\mu\text{m}$ )	HR (PM) or PR(OC) ( $\mu\text{m}$ )	HT ( $\mu\text{m}$ )	HR(PM) or PR(OC) ( $\mu\text{m}$ )	HT ( $\mu\text{m}$ )	HR(PM) or PR(OC) ( $\mu\text{m}$ )
Plane PM	0.8 – 1	1.02 – 1.2 → 99.9%	0.8 – 0.9	1.3 – 1.5 → 99.9%	0.77 – 1.05 1.9 – 2	1.8 – 2.075 (Tm) 2.0 – 2.2 (Ho) <sup>*4</sup>
Plane OC	0.9 – 1	1.064 → 99.5%	0.8 – 0.9	1.36 → 99%	0.77 – 1.05	1.82 - 2.05 → 98.5%
	0.9 – 1	1.064 → 99%				
	0.9 – 1	1.064 → 95%				
	0.9 – 1	1.064 → 90%				
	0.9 – 1	1.064 → 80%				
	0.9 – 1	1.064 → 70%				
Concave OC $R_{OC}$ 25 - 50 - 75 (mm)	0.9 – 1	1.064 → 99%	-	-	0.8 – 1	1.82 – 2.05 → 98.5%
	0.9 – 1	1.064 → 93%				
	0.9 – 1	1.064 → 95%				
	0.9 – 1	1.064 → 90%				
					0.8 – 1	1.82 – 2.05 → 97%
					0.8 – 1	1.82 – 2.05 → 95%
					0.8 – 1	1.82 – 2.05 → 91%
					0.8 – 1	1.82 – 2.05 → 85%

Other optical elements were needed to handle the pump beam or to characterize the output laser emission. Several lenses were used with focal lengths of 10, 30, 50, 75, 100, 150 mm and suitable antireflection coatings from  $\sim 800$  nm up to  $2 \mu\text{m}$ . Several dichroic mirrors were also used to separate two laser wavelengths as well as filters and attenuators, etc.

### 6.3 Crystal holders for cooling

The crystal holders for cooling minimize the heating of the active material and help to dissipate the heat generated in it more efficiently. Good cooling systems reduce losses, improve stability and prevent thermal and mechanical effects by avoiding internal cracks in the crystals. A different set of holders made of copper were used to cool two faces (Figure 3a) and four faces (Figure 3b) of the active medium. Other crystal holders were also designed for different crystal thicknesses (Figure 4). These crystal holders were cooled with water. To improve the thermal contact, a sheet of indium was used.

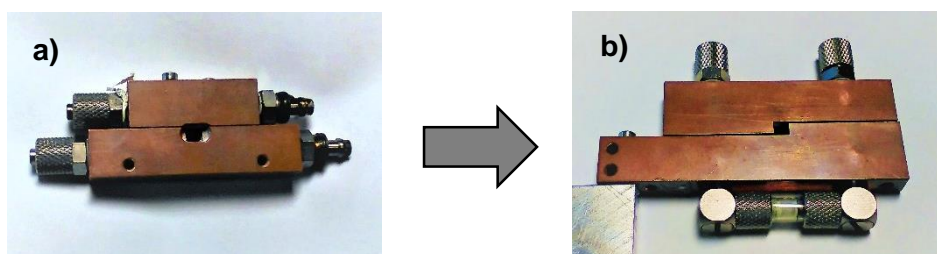


**Figure 3.** a) Cu holder for cooling two faces of the crystals and b) four faces of the crystals

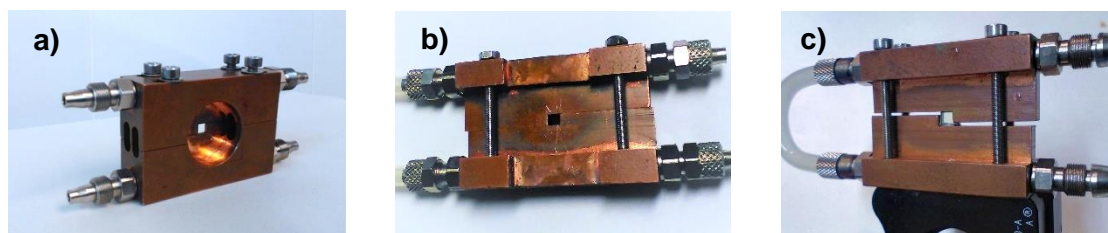


**Figure 4.** Cu holders for cooling four faces of the crystals suitable for different thicknesses of the active media

## 6.4 Cavity setups

The lasers studied here were end-pumped. This means that the pump light is injected parallel to the laser beam. Figure 5 shows the scheme of all the setups used in room temperature conditions. The setups include the laser diode, the optical elements, active material and holder for cooling.

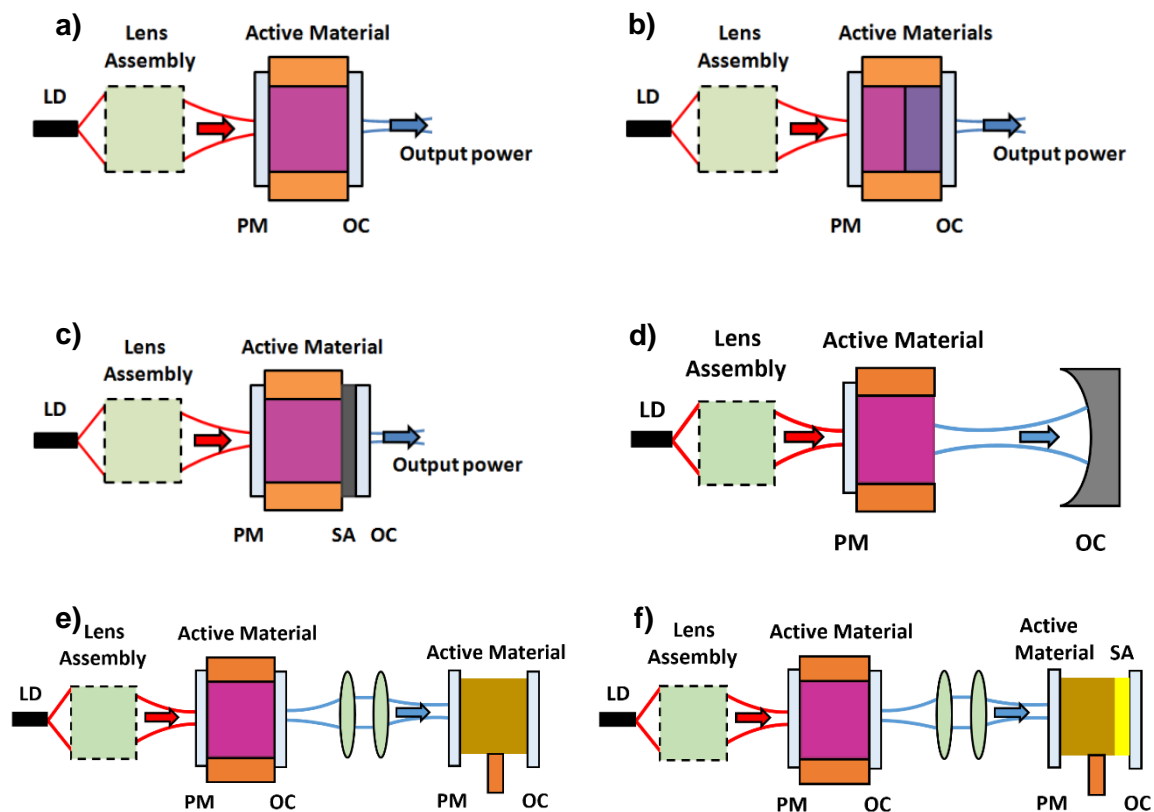


**Figure 5.** Laser setups used in this thesis to generate CW or PQS laser operation. a) Microchip laser with a single active medium, b) microchip intra-cavity pumped laser, c) microchip passive Q-switched laser, d) hemispherical CW configuration, e) in-band pumped CW laser and f) in-band-pumped passive Q-switched laser

## 6.5 External devices

To characterize the laser beam various optical detectors are needed, such as a power meter, spectrometers and a visible-NIR camera in CW. Additionally, in pulsed regime supplementary optical devices are needed to characterize the output beam, such as a fast photo-detector connected to an oscilloscope.

A laser power/energy meter was used to characterize the output beam. It provided good signal stabilization with low noise.

The spectrophotometers were used to detect the laser wavelength emission. Two different devices at different working ranges, from 800 to 1600 nm and from 1000 to 2600 nm, were used with an optical bandpass of  $<0.2$  nm and  $<0.5$  nm, respectively, and a wavelength accuracy of  $\pm 0.2$  nm.

A Near-IR Camera model FIND-R-SCOPE 85706 operating in the 400 – 2000nm region helped to detect the NIR emission, the quality and the laser beam profile. The camera provided high resolution with 25 mm focal f:1.4 manual iris lens. The video image was easily convertible with the help of a computer.

Two different photodetectors were used to detect the single pulses and the pulse train. An InGaAs-PIN photodetector and a Ge-PIN photodetector were used depending on the sensitivity and resolution of each experiment. The InGaAs photodetector had a rise time of  $<200$  ps, a bandwidth of  $>0.3$  GHz and a working spectral range from 800 to 2600 nm (sensitivity value  $>0.5$ ). The Ge photodetector had a rise time of  $<100$  ps, a bandwidth of 3 GHz and a working spectral range from 400 to 2000 nm (sensitivity value  $>0.5$ ). The Ge PIN photodetector was also used at  $2 \mu\text{m}$  because of its high resolution in the determination of a single pulse. The 2 GHz oscilloscope used had a sample rate of 10 GS/s.

## 6.6 Electrospinning setup

The electrospinning experiments were carried out at the DEW (Droplets, intErfaces and floWs) research laboratory belonging to the URV's Department of Engineering. The solution of SWCNTs/PMMA studied is described in [P28]. The setup (see Figure 6) consists of a plastic syringe (5 ml) and a metallic needle of 0.6 mm core diameter cut and polished for a plane tip. The flow was kept constant by the syringe pump at 0.15 ml/h using an infusion syringe pump. A high voltage power supply, maximum  $\pm 15$  kV, was connected parallel to the needle and the black plate. This metallic black plate (with a hole in the middle through which the metallic needle was passed) generated a homogenous electric field which gave better control over nearby objects and oriented the fibres towards the rotatory cylinder. The collector was a 5 cm core diameter rotating at 3000 rpm. The distance between the needle and collector was 5 – 15 cm. The temperature in all experiments was between 20 – 24 °C with a humidity of 30 – 60 %RH.

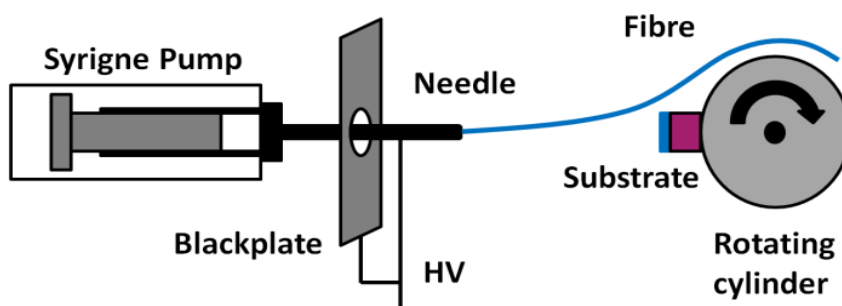


Figure 6. Electrospinning setup for the aligned fibers of SWCNTs/PMMA. HV: High Voltage

## 6.7 Growth, cutting and polishing crystals

The FICMA-FICNA group has considerable experience in growing MDT crystals by the Top-Seeded Solution Growth Slow-Cooling (TSSG-SC) method at high temperature ( $\sim 1000$  °C). This method provides single crystals with a high degree of homogeneity and quality, and without internal cracks. All the MDT crystals studied in this work were grown in the FICMA-

FiCNA laboratories. Other crystals and SAs came from projects with other institutions described in the Preface to this dissertation.

The crystals and SAs were cut and polished with laser quality, flatness and a high parallelism degree between the input and output faces. For cutting, the crystals were fixed with a resin in a goniometer for the desired orientation. A diamond saw disk 0.12 mm thick was used. Once these samples had been cut, they were mounted in a commercial polisher machine for polishing.

## ***6.8 Spectroscopic characterization***

The optical density of the crystals studied and the initial absorption of the SAs were measured with a spectrophotometer, the spectral range of which extended from UV at 175 nm to NIR at 3300 nm. With a variable slit width, the optimum data resolution was 0.01 nm. The equipment took the measurements at room temperature and at low temperature using an external chamber at high vacuum.

To detect the emission of the active ions, two optical spectrum analysers were used with a range detection from 0.4 to 1.2  $\mu\text{m}$  and from 1.2 to 2.4  $\mu\text{m}$ . Both instruments gave resolutions of 0.02 nm (0.4 – 1.2  $\mu\text{m}$ ) and 0.05 nm (1.2 – 2.4  $\mu\text{m}$ ) with high sensitivity.

## ***6.9 Microscopic techniques***

The active materials and SAs were characterized by Environmental Electron Scanning Microscopy (ESEM), Transmission Electron Microscopy (TEM), Raman spectroscopy and X-Ray Diffraction (XRD) at the URV's Science Service.

The ESEM model was a FEI QUANTA 600 with an Energy Dispersive X-ray (EDX) Inca Analyzer (INCAx-sight model 6427) from OXFORD Instruments. The equipment provides beam voltages from 1 kV to 30 kV and can operate in high-vacuum and low-vacuum with a resolution of 1.2 nm and 1.5 nm at 30 kV, respectively. The software is an Inca version 4.01 build 28.

The TEM model was a JEOL TEM-1011. This equipment is a simple, dependable imaging instrument for high throughput of images with excellent contrast definition. The acceleration voltage flexibility is 40 to 100 kV, with 0.2 nm line resolution and 0.4 nm point resolution suitable for thin science specimens. The software imaging is a Megaview 5.1 build 1276.

The Raman spectrometer was a Renishaw inVia Raman microscope, which combines simplicity of operation with high performance and unparalleled flexibility with a spectral resolution better than  $1 \text{ cm}^{-1}$ . The lasers are 514 nm, 633 nm and 785 nm. The software used to treat and collect the data was Wire 4.

The X-ray diffraction patterns were measured with a Siemens EM-1011BU model D5000 X-ray diffractometer. The patterns were obtained using a  $K_{\alpha}$  line copper at  $\lambda = 1.54056 \text{ \AA}$ , which worked with the Bragg-Brentano para-focusing geometry and  $\theta$ - $\theta$  configuration. Moreover, the power diffraction measurements were achieved with a Bruker-AXS D8-Discover with a vertical goniometer equipped with a collimator for the X-ray beam of  $500 \text{ }\mu\text{m}$ . The detector was a GADDS with  $30 \times 30 \text{ cm}^2$  and a  $1024 \times 1024$  pixel CCD sensor. The radiation was achieved by a copper X-ray tube operated at 40 kV and 5 mA.

# References

1. A. L. Schawlow, and C. H. Townes, "Infrared and Optical Masers," *Phys. Rev.*, vol. 112, pp. 1940, 1958.
2. T. H. Maiman, "Stimulated Optical Radiation in Ruby," *Nature*, vol. 187, pp. 493, 1960.
3. M. C. Farries, P. R. Morkel, and J. E. Townsend, "Spectroscopic and lasing characteristics of samarium doped glass fibre," in *IEE Proceedings J. Optoelectronics*, vol. 137, pp. 318, 1990.
4. S. R. Bowman, S. O'Connor, and N. J. Condon, "Diode pumped yellow dysprosium lasers," *Opt. Express*, vol. 20, pp. 12906, 2012.
5. A. Sennaroglu, C. R. Pollock, and H. Nathel, "Efficient continuous-wave chromium-doped YAG laser," *J. Opt. Soc. Am. B*, vol. 12, pp. 930, 1995.
6. S. R. Bowman, J. Ganem, B. J. Feldman, and A. W. Kueny, "Infrared laser characteristics of praseodymium-doped lanthanum trichloride," in *IEEE Journal of Quantum Electronics*, vol. 30, pp. 2925, 1994.
7. D. L. Ross, and J. Blanc, "Europium Chelates as Laser Materials," *Lanthanide/Actinide Chemistry*, pp. 155, 1967.
8. D. W. Coutts, and A. J. S. McGonigle, "Cerium-doped fluoride lasers," in *IEEE Journal of Quantum Electronics*, vol. 40, pp. 1430, 2004.
9. V. Fortin, F. Maes, M. Bernier, S. T. Bah, M. D'Auteuil, and R. Vallée, "Watt-level erbium-doped all-fiber laser at 3.44  $\mu\text{m}$ ," *Opt. Lett.*, vol. 41, pp. 559, 2016.
10. W. Koehler, "Properties of Solid-State Laser Materials," In: *Solid-State Laser Engineering*. Springer Series in Optical Sciences, vol 1, 2006.
11. S. Kostić, Z.Ž. Lazarević, V. Radojević, A. Milutinović, M. Romčević, N.Ž. Romčević, and A. Valčić, "Study of structural and optical properties of YAG and Nd:YAG single crystals," *Materials Research Bulletin*, Vol. 63, pp. 80, 2015.
12. K. Petermann, L. Fornasiero, E. Mix, and V. Peters, "High melting sesquioxides: crystal growth, spectroscopy, and laser experiments," *Optical Materials*, vol. 19, pp. 67, 2002.
13. S. Al-Qaisi, M. S. Abu-Jafar, G. K. Gopir, R. Ahmed, S. B. Omran, R. Jaradat, D. Dahliah, and R. Khenata, "Structural, elastic, mechanical and thermodynamic properties of Terbium oxide: First-principles investigations," *Results in Physics*, vol. 7, pp. 709, 2017.
14. K. Takaichi, H. Yagi, J. Lu, A. Shirakawa, K. Ueda, T. Yanagitani, and A. A. Kaminskii, "Yb<sup>3+</sup> doped Y<sub>3</sub>Al<sub>5</sub>O<sub>12</sub> ceramics - A new solid-state laser material," *Phys. Stat. Sol. (a)*, vol. 200, pp. R5, 2003.
15. S. Radmard, S. Arabgari, and M. Shayganmanesh, "Optimization of Yb:YAG thin-disk-laser design parameters considering the pumping-light back-reflection," *Optics & Laser Technology*, vol. 63, pp. 148, 2014.
16. D. Haliva, T. Ryba, and M. Holzer, "High power disk lasers: advances and Applications," *Proc SPIE*, pp. 8235, 2012.
17. A. Antognini, K. Schuhmann, and F. F. Amaro, "Thin-Disk Yb:YAG Oscillator-Amplifier Laser, ASE, and Effective Yb:YAG Lifetime," in *IEEE Journal of Quantum Electronics*, vol. 45, pp. 993, 2009.
18. K. Scholle, S. Lamrini, P. Koopmann, and P. Fuhrberg, "2  $\mu\text{m}$  Laser Sources and Their Possible Applications, Frontiers in Guided Wave Optics and Optoelectronics," Bishnu Pal (Ed.), InTech, 2010.
19. D. Graham-Rowe, and R. Won, "Lasers for engine ignition," *Nature Photonics*, vol. 2, pp. 515, 2008.
20. F. Dausinger, H. Hugel, and V. I. Konov, "Micromachining with ultrashort laser pulses: from basic understanding to technical applications," *Proc. SPIE 5147, ALT'02 International Conference on Advanced Laser Technologies*, 2003.
21. H. Kikuta, "Distance measurement by the wavelength shift of laser diode light", *Appl. Opt.*, vol. 25, pp. 2976, 1986.
22. G. Beheim, and K. Fritsch, "Range finding using frequency-modulated laser diode", *Appl. Opt.*, vol. 25, pp. 1439, 1986.

23. A. Gaspar, H. Brandi, V. Gomez, and D. Luque, "Efficacy of Erbium:YAG laser treatment compared to topical estriol treatment for symptoms of genitourinary syndrome of menopause," *Lasers Surg. Med.*, vol. 49, pp. 160, 2017.
24. J. Yu, U. N. Singh, J. C. Barnes, N. P. Barnes, and M. Petros, "An efficient double-pulsed 2-micron laser for DIAL applications," *Advances in Laser Remote Sensing*, pp. 53, 2000.
25. M. H. Niemz "Laser - Tissue Interactions," Springer, Berlin, 2007.
26. L. C. Martens, "Laser physics and a review of laser applications in dentistry for children," *European Archives of Paediatric Dentistry*, vol. 12, pp. 61, 2011.
27. F. J. McClung, and R. W. Hellwarth, "Giant optical pulsations from ruby," *J. Appl. Phys.*, vol. 33, pp. 828, 1962.
28. J. J. Degnan, "Optimization of passively Q-switched lasers," *IEEE J. Quantum Electron.*, vol. 31, pp. 1890, 1995.
29. G. J. Spühler, "Experimentally confirmed design guidelines for passively Q-switched microchip lasers using semiconductor saturable absorbers," *J. Opt. Soc. Am. B*, vol. 16, pp. 376, 1999.
30. I. C. Chang, "Acousto-Optic Devices and Applications," *IEEE Trans. On Sonics and Ultrasonic*, vol. 1, pp. 1, 1976.
31. A. E. Siegman, "Lasers," Oxford University Press, 1986.
32. A. F. El-Sherif, "High Performance of a Mechanical Q-switched Tm<sup>3+</sup> doped silica Fiber Laser Operating near 2  $\mu\text{m}$ ," 2nd International Conference on Engineering Mathematics and Physics (EMP-2), vol. 23, pp. 65, 2004.
33. Y. M. Chang, J. Lee, Y. Jhon, and J. H. Lee, "Active Q-switching in an erbium-doped fiber laser using an ultrafast silicon-based variable optical attenuator," *Opt. Express*, vol. 19, pp. 26911, 2011.
34. B. K. Garside, and T. K. Lim, "Laser mode locking using saturable absorbers," *J. Appl. Phys.*, vol. 44, pp. 2335, 1973.
35. A. Sennaroglu, "Continuous wave thermal loading in saturable absorbers: theory and experiment," *Appl. Opt.*, vol. 36, pp. 9528, 1997.
36. G. J. Spühler, R. Paschotta, R. Fluck, B. Braun, M. Moser, G. Zhang, E. Gini, and U. Keller, "Experimentally confirmed design guidelines for passively Q-switched microchip lasers using semiconductor saturable absorbers," *J. Opt. Soc. Am. B*, vol. 18, pp. 886, 2001.
37. Y. P. Chen, Y. P. Lan, and H. L. Chang, "Analytical model for design criteria of passively Q-switched lasers," in *IEEE Journal of Quantum Electronics*, vol. 37, pp. 462, 2001.
38. Z. Burshtein, "Excited-state absorption studies of Cr<sup>4+</sup> ions in several garnet host crystals," *IEEE J. Quantum Electron.*, vol. 34, pp. 292, 1998.
39. A. V. Podlipensky, V. G. Shcherbitsky, N. V. Kuleshov, V. P. Mikhailov, V. I. Levchenko, and V. N. Yakimovich, "Cr<sup>2+</sup>:ZnSe and Co<sup>2+</sup>:ZnSe saturable-absorber Q switches for 1.54- $\mu\text{m}$  Er:glass lasers," *Opt. Lett.*, vol. 24, pp. 960, 1999.
40. A. Fuerbach, X. Jiang, and S. Gross, "Novel nanomaterial-based saturable absorbers for ultrashort-pulsed mid-infrared waveguide chip lasers," 2016 18th International Conference on Transparent Optical Networks (ICTON), Trento, pp. 1, 2016.
41. Q. Bao, H. Zhang, Y. Wang, Z. Ni, Y. Yan, Z. X. Shen, K. P. Loh, and D.Y. Tang, "Atomic-Layer Graphene as a Saturable Absorber for Ultrafast Pulsed Lasers," *Adv. Funct. Mater.*, vol. 19, pp. 3077, 2009.
42. G. Zheng, Y. Chen, H. Huang, C. Zhao, S. Lu, S. Chen, H. Zhang, and S. Wen, "Improved Transfer Quality of CVD-Grown Graphene by Ultrasonic Processing of Target Substrates: Applications for Ultra-fast Laser Photonics," *ACS Applied Materials & Interfaces*, vol. 5, pp. 10288, 2013.
43. I. H. Baek, S. Y. Choi, H. W. Lee, W. B. Cho, V. Petrov, A. Agnesi, V. Pasiskevicius, D. Yeom, K. Kim, and F. Rotermund, "Single-walled carbon nanotube saturable absorber assisted high-power mode-locking of a Ti:sapphire laser," *Opt. Express*, vol. 19, pp. 7833, 2011.
44. G. Sobon, J. Sotor, I. Pasternak, A. Krajewska, W. Strupinski, and K. M. Abramski, "Multilayer graphene-based saturable absorbers with scalable modulation depth for mode-locked Er- and Tm-doped fiber lasers," *Opt. Mater. Express*, vol. 5, pp. 2884, 2015.

45. D. Li, H. Jussila, L. Karvonen, G. Ye, H. Lipsanen, X. Chen, and Z. Sun, "Polarization and Thickness Dependent Absorption Properties of Black Phosphorus: New Saturable Absorber for Ultrafast Pulse Generation," *Scientific Reports*, vol. 5, pp. 15899, 2015.
46. G. Sobon, A. Duzynska, M. Świniarski, J. Judek, J. Sotor, and M. Zdrojek, "CNT-based saturable absorbers with scalable modulation depth for Thulium-doped fiber lasers operating at 1.9  $\mu\text{m}$ ," *Sci Rep.*, vol. 7, pp. 45491, 2017.
47. M. Chen, Y. Zhu, Y. Pan, H. Kou, H. Xu, and J. Guo, "Gradient multilayer structural design of CNTs/SiO composites for improving microwave absorbing properties," *Materials & Design*, vol. 32, pp. 3013, 2011.
48. J. J. Zayhowski, "Q-switched operation of microchip lasers," *Opt. Lett.*, vol. 16, pp. 575, 1991.
49. J. J. Zayhowski, and A. Mooradian, "Single-frequency microchip Nd lasers," *Opt. Lett.*, vol. 14, pp. 24, 1989.
50. J. J. Zayhowski, "Passively Q-switched microchip lasers and Applications," *Rev. Laser Eng.*, vol. 26, pp. 841, 1998.
51. J. J. Zayhowski, "Gain-switched pulsed operation of microchip lasers," *Opt. Lett.*, vol. 14, pp. 1318, 1989.
52. D. G. Matthews, N. MacKinnon, R. S. Conroy, and B. D. Sinclair, "Blue microchip laser fabricated from Nd:YAG and  $\text{KNbO}_3$ ," *Opt. Lett.*, vol. 21, pp. 198, 1996.
53. N. J. van Druten, S. S. R. Oemrawsingh, Y. Lien, C. Serrat, M. P. van Exter, and J. P. Woerdman, "Observation of transverse modes in a microchip laser with combined gain and index guiding," *J. Opt. Soc. Am. B*, vol. 18, pp. 1793, 2001.
54. C. A. Wang, and S. H. Groves, "New materials for diode laser pumping of solid-state lasers," *IEEE J. Quantum Electron*, vol. 28, pp. 942, 1992.
55. P. J. Delfyett et al., "High-power ultrafast laser diodes," *IEEE J. Quantum Electron*, vol. 28, pp. 2203, 1992.
56. L. A. Coldren, and S. W. Corzine, "Diode Lasers and Photonic Integrated Circuits," John Wiley & Sons, New York, 1995.
57. W. W. Chow, and S. W. Koch, "Semiconductor-Laser Fundamentals," Springer, Berlin, 1999.
58. F. Welch, "A brief history of high-power semiconductor lasers," in *IEEE Journal of Selected Topics in Quantum Electronics*, vol. 6, pp. 1470, 2000.
59. C. Whipple, "Microchip Laser Nears 2-MW Output," *SPIE Newsroom*, pp. 7, 2005.
60. R. Bhandari, and T. Taira, "Megawatt level UV output from [110]  $\text{Cr}^{4+}$ :YAG passively Q-switched microchip laser," *Opt. Express* vol. 19, pp. 22510, 2011.
61. R. Paschotta et al., "Passively Q-switched 0.1 mJ fiber laser system at 1.53  $\mu\text{m}$ ," *Opt. Lett.*, vol. 24, pp. 388, 1999.
62. L. E. Holder et al., "One joule per Q-switched pulse diode-pumped laser," *IEEE J. Quantum Electron*, vol. 28, pp. 986, 1992.
63. Ross, V., et al., "Comparison of Responses of Tattoos to Picosecond and Nanosecond Q-switched Neodymium-YAG lasers," *Arch Dermatol*, vol. 134, pp. 167, 1991.
64. M. E. Fermann, A. Galvanauskas, and G. Sucha, "Ultrafast Lasers: Technology and Applications," Marcel Dekker, New York, 2003.
65. V. Ashoori, M. Shayganmanesh, and S. Radmard, "Heat Generation and Removal in Solid State Lasers, An Overview of Heat Transfer Phenomena," Dr M. Salim Newaz Kazi (Ed.), InTech, 2012.
66. V. Jambunathan, X. Mateos, M. C. Pujol, J. J. Carvajal, U. Griebner, V. Petrov, M. Aguiló, and F. Díaz, "Diode-pumped continuous-wave laser operation of co-doped (Ho,Tm):KLu(WO<sub>4</sub>)<sub>2</sub> monoclinic crystal," *Optics & Laser Technology*, vol. 54, pp. 326, 2013.
67. K. Wang, and J. Wang, "Spectroscopic properties of ytterbium doped KLu(WO<sub>4</sub>)<sub>2</sub>," *Journal of Rare Earths*, vol. 29, pp. 359, 2011.
68. C. Zhang, Z. Li, H. Cong, J. Wang, H. Zhang, and R.I. Boughton, "Crystal growth and thermal properties of single crystal monoclinic NdCOB (NdCa<sub>4</sub>O(BO<sub>3</sub>)<sub>3</sub>)," *Journal of Alloys and Compounds*, vol 507, pp. 335, 2010.
69. H. Cong, H. Zhang, S. Sun, Y. Yu, W. Yu, H. Yu, J. Zhang, J. Wang, and R. I. Boughton, "Morphological study of Czochralski-grown lanthanide orthovanadate single crystals and implications on the mechanism of bulk spiral formation," *Journal of Applied Crystallography*, vol. 43, pp. 308, 2010.

70. V. Petrov, M. C. Pujol, X. Mateos, Ó. Silvestre, S. Rivier, M. Aguiló, R. M. Solé, J. Liu, U. Griebner, and F. Díaz, "Growth and properties of  $\text{KLu}(\text{WO}_4)_2$ , and novel ytterbium and thulium lasers based on this monoclinic crystalline host," *Laser & Photon. Rev.*, vol. 1, pp. 179, 2007.
71. D.R. Lovett, "Tensor properties of Crystals," IOP publishing 2on Edition, 1999.
72. B. R. Judd, "Optical absorption intensities of rare earth ions," *Phys. Rev.*, vol. 127, pp. 750, 1962.
73. A. J. Kenyon, "Recent developments in rare-earth doped materials for optoelectronics," *Prog. Quantum Electron*, vol. 26, pp. 225, 2002.
74. J. Liu, W. Han, H. Zhang, J. Wang, and V. Petrov, "Comparison of laser performance of  $\text{Yb:YCa}_4\text{O}(\text{BO}_3)_3$  crystals cut along the principal optical axes," *Applied Physics B*, vol. 91, pp. 329, 2008.
75. S. F. Chénais, F. Druon, P. Balembois, A. Georges, G. Brenier, and G. Boulon, "Diode-pumped Yb:GGG laser: comparison with Yb:YAG," *Optical Materials*, vol. 22, pp. 99, 2003.
76. P. H. Haumesser, R. Gaumé, B. Viana, E. A. Fidancev, and D. Vivien, "Spectroscopic and crystal-field analysis of new Yb-doped laser materials," *J. Phys. Condens. Matter*, vol. 13, pp. 5427, 2001.
77. F. Pirzio, E. Caracciolo, S. D. D. D. Cafiso, M. Kemnitzer, A. Guandalini, F. Kienle, S. Veronesi, M. Tonelli, J. A. d. Au, and A. Agnesi, "Ultrafast Solid-State Oscillators and High-Power Amplifiers Based on Broadband, Multisite Yb-doped Crystals," *European Conference on Lasers and Electro-Optics - European Quantum Electronics Conference*, paper CA\_2\_1, 2015.
78. A. A. Demidovich, A. P. Shkadarevich, M. B. Danailov, P. Apai, T. Gasmi, V. P. Gribkovskii, A. N. Kuzmin, G. I. Ryabtsev, and L. E. Batay, "Comparison of cw laser performance of Nd:KGW, Nd:YAG, Nd:BEL, and Nd:YVO<sub>4</sub> under laser diode pumping," *Applied Physics B*, vol. 67, pp. 11, 1998.
79. T. Graf, and J. E. Balmer, "Lasing Properties of Diode Laser-Pumped Nd:KGW," in *Advanced Solid State Lasers*, OSA Proceedings Series, vol. 24, LM5, 1995.
80. F. J. Bruni, "Growth of Nd:YAG and Cr, Nd:GScGG A Comparative Study," *Tunable Solid State Lasers for Remote Sensing*, pp. 123, 1985.
81. J. B. Gruber, D. K. Sardara, K. L. Nash, and R. M. Yow, "Comparative study of the crystal-field splitting of trivalent neodymium energy levels in polycrystalline ceramic and nanocrystalline yttrium oxide," *Journal of Applied Physics*, vol. 102, pp. 023103, 2007.
82. J. E. Geusic et al., "Laser oscillations in Nd-doped yttrium aluminium, yttrium gallium and gadolinium garnets," *Appl. Phys. Lett.*, vol. 4, pp. 182, 1964.
83. M.C. Pujol, X. Mateos, A. Aznar, X. Solans, S. Suriñac, J. Massons, F. Díaz, and M. Aguiló, "Structural redetermination, thermal expansion and refractive indices of  $\text{KLu}(\text{WO}_4)_2$ ," *J. Appl. Cryst.*, vol. 39, pp. 230, 2006.
84. M.C. Pujol, X. Mateos, R. Solé, J. Massons, Jna. Gavalda, F. Díaz and M. Aguiló, "Linear thermal expansion tensor in  $\text{KRE}(\text{WO}_4)_2$  (RE = Gd, Y, Er and Yb) monoclinic crystals," *Materials Science Forum*, pp. 378, 2001.
85. Ó. Silvestre, J. Grau, M. C. Pujol, J. Massons, M. Aguiló, F. Díaz, M. T. Borowiec, A. Szewczyk, M. U. Gutowska, M. Massot, A. Salazar and V. Petrov "Thermal properties of monoclinic  $\text{KLu}(\text{WO}_4)_2$  as a promising solid-state laser host," *Opt. Express*, vol. 16, pp. 5022, 2008.
86. M. J. Weber, "Handbook of optical materials," CRC press, 2003.
87. A. A. Kaminski, "Laser Crystals," *Springer Series in Optical Sciences*, 1981.
88. K. Walter, "Solid-State Laser Engineering," *Springer-Verlag*, 1992.
89. M. Guzik, J. Pejchal, A. Yoshikawa, A. Ito, T. Goto, M. Siczek, T. Lis, and G. Boulon, "Structural Investigations of  $\text{Lu}_2\text{O}_3$  as Single Crystal and Polycrystalline Transparent Ceramic," *Crystal Growth & Design*, vol. 14, pp. 3327, 2014.
90. C. Kränkel, "Rare-Earth-Doped Sesquioxides for Diode-Pumped High-Power Lasers in the 1-, 2-, and 3- $\mu\text{m}$  Spectral Range," in *IEEE Journal of Selected Topics in Quantum Electronics*, vol. 21, pp. 250, 2015.
91. D. Dimitrov, P. Rafailov, V. Marinova, T. Babeva, E. Goovaerts, Y. Chen, C. S Lee, and J. Juang, "Structural and optical properties of  $\text{LuVO}_4$  single crystals," *Journal of Physics: J. Phys.: Conf. Ser.* 794 012029, 2017.
92. S. Zhao, H. Zhang, Y. Lu, J. Liu, J. Wang, X. Xu, H. Xia, and M. Jiang, "Spectroscopic characterization and laser performance of Nd:LuVO<sub>4</sub> crystal," *Opt. Materials*, vol. 28, pp. 950, 2006.
93. S. A. Miller, H. E. Rast, and H. H. Caspers, "Lattice vibrations of  $\text{LiYF}_4$ ," *J. Chem. Phys.*, vol. 52, pp. 4172, 1970.

94. I. Razumova, A. Tkachuk, A. Nikitichev, and D. Mironov, "Spectral-luminescent properties of Tm:YLF crystal," *Journal of Alloys and Compounds*, vol. 225, pp. 129, 1995.
95. F. P. Yu et al, "Rare-Earth Calcium Oxyborate Piezoelectric Crystals  $\text{ReCa}_4\text{O}(\text{BO}_3)_3$ . Growth and Piezoelectric Characterizations," *Crystals*, vol. 4, pp. 241, 2014.
96. A. Aron et al., "Spectroscopic properties and laser performances of Yb:YCOB and potential of the Yb:LaCOB material," *Opt. Mater.*, vol. 16, pp. 181, 2001.
97. H. Liu, X. Chen, X. Huang, X. Xu, G. Zhang, and N. Ye, "Growth and optical properties of UV transparent YAB crystals," *Materials Research Innovations*, vol. 15, pp. 140, 2011.
98. P. Wang, J. M. Dawes, P. Dekker, D. S. Knowles, J. A. Piper, and B. Lu, "Growth and evaluation of ytterbium-doped yttrium aluminium borate as a potential self-doubling laser crystal," *J. Opt. Soc. Am. B*, vol. 16, pp. 63, 1999.
99. A. A. Kaminskii, "Laser crystals and ceramics: recent advances," *Laser Photonics Rev.*, vol. 1, pp. 93, 2007.
100. A. Y. Zaouter, J. Didierjean, F. Balambois, G. Lucas Leclin, F. Druon, P. Georges, J. Petit, P. Goldner, and B. Viana, "47-fs diode-pumped  $\text{Yb}^{3+}:\text{CaGdAlO}_4$  laser," *Optics Letters*, vol. 31, pp. 119, 2006.
101. J. Petit, P. Goldner, and B. Viana, "Laser emission with low quantum defect in  $\text{Yb}:\text{CaGdAlO}_4$ ," *Opt. Lett.*, vol. 30, pp. 1345, 2005.
102. E. Cavalli, A. Belletti, and M. G. Brik, "Optical spectra and energy levels of the Cr ions in MWO (M=Mg, Zn, Cd) and  $\text{MgMoO}$  crystals," *Journal of Physics and Chemistry of Solids*, vol. 69, pp. 29, 2008.
103. L. Zhang, Y. Huang, S. Sun, F. Yuan, Z. Lin, and G. Wang, "Thermal and spectral characterization of Cr:MgWO—a promising tunable laser material," *Journal of Luminescence*, vol. 169, pp. 161, 2016.
104. N. Krutyak, V. V. Mikhailin, D. Spassky, I. A. Tupitsyna, and A. M. Dubovik, "Luminescent properties of  $\text{MgWO}_4$  crystals," *IEEE International Conference on Oxide Materials for Electronic Engineering*, Lviv, Ukraine, pp. 235, 2012.
105. J. M. Cano-Torres, X. Han, A. García-Cortés, M. D. Serrano, C. Zaldo, F.J. Valle, X. Mateos, S. Rivier, U. Griebner, and V. Petrov, "Infrared spectroscopic and laser characterization of Tm in disordered double Tungstates," *Materials Science and Engineering B*, vol. 146, pp. 22, 2008.
106. J. M. Cano-Torres, M. D. Serrano, C. Zaldo, M. Rico, X. Mateos, J. Liu, U. Griebner, V. Petrov, F. J. Valle, M. Galán, and G. Viera, "Broadly tunable laser operation near  $2\mu\text{m}$  in a locally disordered crystal of  $\text{Tm}^{3+}$ -doped  $\text{NaGd}(\text{WO}_4)_2$ ," *J. Opt. Soc. Am. B*, vol. 23, pp. 2494, 2006.
107. S. E. Ivanova, A. M. Tkachuk, A. Mirzaeva, and F. Pellé, "Spectroscopic study of thulium-activated double sodium yttrium fluoride  $\text{Na}_{0.4}\text{Y}_{0.6}\text{F}_{2.2}:\text{Tm}^{3+}$  crystals: I. Intensity of spectra and luminescence kinetics," *Optics spectroscopy*, vol. 105, pp. 228, 2008.
108. O. Silvestre, M. C. Pujol, M. Rico, F. Güell, M. Aguiló, and F. Díaz, "Thulium doped monoclinic  $\text{KLu}(\text{WO}_4)_2$  single crystals: growth and spectroscopy," *Applied Physics B*, vol. 87, pp. 707, 2007.
109. Y. Kalisky, J. Kagan, and D. Sagie, "Spectroscopic properties, energy transfer, and laser operation of pulsed holmium lasers," *Journal of Applied Physics*, vol. 70, pp. 4095, 1991.
110. G. J. Vassar, J. M. Teichman, and R. D. Glickman, "Holmium:YAG lithotripsy efficiency varies with energy density," *J. Urol.*, vol. 160, pp. 471, 1998.
111. P. J. Morris, W. Lüthy, H. P. Weber, S. Y. Rusanov, A. I. Zagumenyi, I. A. Shcherbakov, and A. F. Umyskov, "Is a cw  $3\mu\text{m}$  holmium laser possible? A spectroscopic study," *Journal of Quantitative Spectroscopy and Radiative Transfer*, vol. 52, pp. 545, 1994.
112. X. Mateos, F. Di Trapani, V. Petrov, U. Griebner, M. Aguiló, and F. Díaz, "Efficient diode-pumped Tm,Ho:KLuW laser," *Conference on Lasers and Electro-Optics (CLEO) - Laser Science to Photonic Applications*, San Jose, CA, pp. 1, 2014.
113. F. X. Hartmann, and S. R. Rotman, "Energy transfer by the exchange interaction in non-uniform codoped solid-state crystals," *Chemical Physics Letters*, vol. 163, pp. 437, 1989.
114. M. Okida, M. Itoh, T. Yatagai, H. Ogilvy, J. Piper, and T. Omatsu, "Heat generation in Nd doped vanadate crystals with 1.34  $\mu\text{m}$  laser action," *Opt. Express*, vol. 13, pp. 4909, 2005.

115. P. A. Loiko, K. V. Yumashev, N. V. Kuleshov, G. E. Rachkovskaya, and A. A. Pavlyuk, "Thermo-optic dispersion formulas for monoclinic double tungstates  $KRe(WO_4)_2$  where  $Re=Gd, Y, Lu, Yb$ ," In *Optical Materials*, vol. 33, pp. 1688, 2011.
116. V. G. Savitski et al., "The prospects for Yb- and Nd-doped tungstate microchip lasers," 2013 Conference on Lasers & Electro-Optics Europe & International Quantum Electronics Conference, Munich, pp. 1, 2013.
117. J. K. Jabczynski, J. Jaguo, W. Endzian, and J. Kwiatkowski, "Thermo-optic effects in solid state lasers end-pumped by fiber coupled diodes," *Opto-electronics Review*, vol. 13, 2005.
118. M. Shayganmanesh, M.H. Daemi, Zh. Osgoui, S. Radmard, and S.Sh. Kazemi, "Measurement of thermal lensing effects in high power thin disk laser," *Optics & Laser Technology*, vol. 44, pp. 2292, 2012.
119. P. A. Loiko, I. A. Denisov, K. V. Yumashev, N. V. Kuleshov, and A. A. Pavlyuk, "Laser performance and thermal lensing in flashlamp pumped Np-cut and Ng-cut Nd:KGW crystals," *Appl Phys B*, vol. 100, pp. 477, 2010.
120. J. Petit, "Monocristaux dopés ytterbium et matériaux assemblés pour lasers de fortes puissances," PhD Chimie Paritech, 2006.
121. P. Loiko, F. Druon, P. Georges, B. Viana, and K. Yumashev, "Thermo-optic characterization of Yb:CaGdAlO<sub>4</sub> laser crystal," *Opt. Mater. Express*, vol. 4, pp. 2241, 2014.
122. O. Silvestre, J. Grau, M. Pujol, J. Massons, M. Aguiló, F. Díaz, M. Borowiec, A. Szewczyk, M. Urszula Gutowska, M. Massot, A. Salazar, and V. Petrov, "Thermal properties of monoclinic KLu(WO<sub>4</sub>)<sub>2</sub> as a promising-solid state laser host," *Optics express*, vol. 16, pp. 5022, 2008.
123. V. Cardinali, E. Marmois, B. Le Garrec, and G. Bourdet, "Determination of the Thermo-Optic Coefficient  $dn/dT$  of Ytterbium Doped Ceramics ( $Sc_2O_3, Y_2O_3, Lu_2O_3, YAG$ ), Crystals (YAG, CaF<sub>2</sub>) and Neodymium Doped Phosphate Glass at Cryogenic Temperature," *Optical Materials*, vol. 34, pp. 990, 2012.
124. S. Chénais, F. Druon, S. Forget, F. Balembos, and P. Georges, "On thermal effects in solid-state lasers: The case of ytterbium-doped materials," *Prog. Quantum Electron*, vol. 30, pp. 89, 2006.
125. P.A. Loiko, K.V. Yumashev, R. Schödel, M. Pletz, C. Liebald, X. Mateos, B. Deppe, and C. Kränkel, "Thermo-optic properties of Yb:Lu<sub>2</sub>O<sub>3</sub> single crystal," *Appl. Phys. B*, vol. 120, pp. 601, 2015.
126. P. A. Loiko, K. V. Yumashev, V. N. Matrosov, and N. V. Kuleshov, "Dispersion and anisotropy of thermos-optic coefficients in tetragonal GdVO<sub>4</sub> and YVO<sub>4</sub> laser host crystals," *Appl. Opt.*, vol. 52, pp. 698, 2013
127. Y. Sato, and T. Taira, "The studies of thermal conductivity in GdVO<sub>4</sub>, YVO<sub>4</sub>, and Y<sub>3</sub>Al<sub>5</sub>O<sub>12</sub> measured by quasi-one-dimensional flash method," *Opt. Express*, vol. 14, pp. 10528, 2006.
128. B. Denker, and E. Shklovshy, "Handbook of Solid-State Lasers: Materials, Systems and Applications," Woodhead Published Limited, 2013.
129. A. Pirri, D. Alderighi, G. Toci, M. Vannini, M. Nikl, and H. Sato, "Direct Comparison of Yb<sup>3+</sup>:CaF<sub>2</sub> and heavily doped Yb<sup>3+</sup>:YLF as laser media at room temperature," *Optics express*, vol. 17, pp. 18312, 2009.
130. P. Loiko, X. Mateos, Y. Wang, Z. Pan, K. Yumashev, H. Zhang, U. Griebner, and V. Petrov, "Thermo-optic dispersion formulas for YCOB and GdCOB laser host crystals," *Opt. Mater. Express*, vol. 5, pp. 1089, 2015.
131. P. A. Loiko, V. V. Filippov, N. V. Kuleshov, N. I. Leonyuk, V. V. Maltsev, and K. V. Yumashev, "Thermo-optic characterization of Yb:YAl<sub>3</sub>(BO<sub>3</sub>)<sub>4</sub>," *Appl. Phys. B*, vol. 117, pp. 577, 2014.
132. R. J. Aggarwal, D. R. Ripin, J. Ochoa, and T. Y. Fan, "Measurement of thermo-optic properties of Y<sub>3</sub>Al<sub>5</sub>O<sub>12</sub>, Lu<sub>3</sub>Al<sub>5</sub>O<sub>12</sub>, YAlO<sub>3</sub>, LiYF<sub>4</sub>, LiLuF<sub>4</sub>, BaY<sub>2</sub>F<sub>8</sub>, KGd(WO<sub>4</sub>)<sub>2</sub>, and KY(WO<sub>4</sub>)<sub>2</sub> laser crystals in the 80-300 K temperature range," *Journal of Applied Physics*, vol. 98, pp. 103514, 2005.
133. A. E. Siegman, "Analysis of laser beam quality degradation caused by quartic phase aberrations," *Appl. Opt.*, vol. 32, pp. 5893, 1993.
134. F. X. Kaertner, "Ultrafast Optics: Chapter 4 - laser dynamics," Spring Term, 2005.
135. M. Hercher, "An Analysis of Saturable Absorbers," *Appl. Opt.*, vol. 6, pp. 947, 1967.
136. H. Zhang, S. B. Lu, J. Zheng, J. Du, S. C. Wen, D. Y. Tang, K. P. Loh, "Molybdenum disulfide (MoS<sub>2</sub>) as a broadband saturable absorber for ultra-fast photonics," *Opt. Express*, vol. 22, pp. 7249, 2014.

- 
137. J. Du, Q. K. Wang, G. B. Jiang, C. W. Xu, C. J. Zhao, Y. J. Xiang, and Y. Chen, "Ytterbium-doped fiber laser passively mode locked by few-layer molybdenum disulfide ( $\text{MoS}_2$ ) saturable absorber functioned with evanescent field interaction," *Sci. Rep.*, vol. 4, pp. 6346, 2014.
  138. Y. Kalisky, "Cr-doped crystals: their use as lasers and passive Q-switches," *Progress in Quantum Electronics*, vol. 28, pp. 249, 2004.
  139. A. M. Malyarevich et al., "V:YAG - a new passive Q-switch for diode-pumped solid-state lasers," *Appl. Phys. B*, vol. 67, pp. 555, 1998.
  140. D. M. Simanovskii, H. A. Schwettman, H. Lee, and A. J. Welch, "Midinfrared optical breakdown in transparent dielectrics," *Phys. Rev. Lett.*, vol. 91, pp. 107601, 2003.
  141. U. Keller et al., "Semiconductor saturable absorber mirrors (SESAMs) for femtosecond to nanosecond pulse generation in solid-state lasers," *IEEE J. Sel. Top. Quantum Electron*, vol. 2, pp. 435, 1996.
  142. U. Keller, "Semiconductor nonlinearities for solid-state laser modelocking and Q-switching," in *Semiconductors and Semimetals*, Vol. 59A, 1999.
  143. M. Segura, X. Mateos, M. C. Pujol, J. J. Carvajal, V. Petrov, M. Aguiló, and F. Díaz, "CW laser operation around 2- $\mu\text{m}$  in (Tm,Yb):KLu( $\text{WO}_4$ )<sub>2</sub>," *Physics Procedia*, vol. 8, pp. 157, 2010.



## List of Publications

Because of editorial policies on copyright, the publications can be downloaded from the webpage of each journal. The results obtained in this study are published in **indexed international journals**:

- [P1] P. A. Loiko, **J. M. Serres**, X. Mateos, K. V. Yumashev, N. V. Kuleshov, V. Petrov, U. Griebner, M. Aguiló, and F. Díaz, "**Characterization of the thermal lens in 3at. %Tm:KLu(WO<sub>4</sub>)<sub>2</sub> and microchip laser operation**," Laser Phys. Lett., vol. 11, pp. 075001, 2014.  
<https://doi.org/10.1088/1612-2011/11/7/075001>
- [P2] **J. M. Serres**, X. Mateos, P. Loiko, K. Yumashev, N. Kuleshov, V. Petrov, U. Griebner, M. Aguiló, and F. Díaz, "**Diode-pumped microchip Tm:KLu(WO<sub>4</sub>)<sub>2</sub> laser with more than 3 W of output power**," Opt. Lett., vol. 39, pp. 4247, 2014.  
<https://doi.org/10.1364/OL.39.004247>
- [P3] P. A. Loiko, **J. M. Serres**, X. Mateos, K. V. Yumashev, N. V. Kuleshov, V. Petrov, U. Griebner, M. Aguiló, and F. Díaz, "**Thermal lensing in Yb:KLu(WO<sub>4</sub>)<sub>2</sub> crystals cut along the optical indicatrix axes**," Laser Phys. Lett., vol. 11, pp. 125802, 2014.  
<https://doi.org/10.1088/1612-2011/11/12/125802>
- [P4] P. Loiko, **J. M. Serres**, X. Mateos, K. Yumashev, N. Kuleshov, V. Petrov, U. Griebner, M. Aguiló, and F. Díaz, "**Microchip laser operation of Tm,Ho:KLu(WO<sub>4</sub>)<sub>2</sub> crystal**," Opt. Express, vol. 22, pp. 1415, 2014.  
<https://doi.org/10.1364/OE.22.027976>
- [P5] P. Loiko, **J. M. Serres**, X. Mateos, K. Yumashev, N. Kuleshov, V. Petrov, U. Griebner, M. Aguiló, and F. Díaz, "**In-band-pumped Ho:KLu(WO<sub>4</sub>)<sub>2</sub> microchip laser with 84 % slope efficiency**," Opt. Lett., vol. 40, pp. 344, 2015.  
<https://doi.org/10.1364/OL.40.000344>
- [P6] **J. M. Serres**, P. Loiko, X. Mateos, K. Yumashev, N. Kuleshov, V. Petrov, U. Griebner, M. Aguiló, and F. Díaz, "**Prospects of monoclinic Yb:KLu(WO<sub>4</sub>)<sub>2</sub> crystal for multi-watt microchip lasers**," Opt. Mater. Express, vol. 5, pp. 661, 2015.  
<https://doi.org/10.1364/OME.5.000661>

- 
- [P7] **J. M. Serres**, P. A. Loiko, X. Mateos, K. V. Yumashev, N. V. Kuleshov, V. Petrov, U. Griebner, M. Aguiló, and F. Díaz, “**Ho:KLuW microchip laser intracavity pumped by a diode-pumped Tm:KLuW laser**,” *Appl. Phys. B*, vol. 120, pp. 123, 2015.  
<https://doi.org/10.1007/s00340-015-6112-2>
- [P8] **J. M. Serres**, P. Loiko, X. Mateos, K. Yumashev, U. Griebner, V. Petrov, M. Aguiló, and F. Díaz, “**Tm:KLu(WO<sub>4</sub>)<sub>2</sub> microchip laser Q-switched by a graphene-based saturable absorber**,” *Opt. Express*, vol. 23, pp. 14108, 2015.  
<https://doi.org/10.1364/OE.23.014108>
- [P9] **J. M. Serres**, X. Mateos, U. Griebner, V. Petrov, M. Aguiló, and F. Díaz, “**Single-layer graphene saturable absorber for diode-pumped passively Q-switched Tm:KLu(WO<sub>4</sub>)<sub>2</sub> laser at 2 μm**,” *Laser Phys. Lett.*, vol. 12, pp. 095802, 2015.  
<https://doi.org/10.1088/1612-2011/13/2/025801>
- [P10] P. Loiko, **J. M. Serres**, X. Mateos, K. Yumashev, A. Malyarevich, A. Onushchenko, V. Petrov, U. Griebner, M. Aguiló, and F. Díaz, “**Ho:KLu(WO<sub>4</sub>)<sub>2</sub> Microchip Laser Q-Switched by a PbS Quantum-Dot-Doped Glass**,” *IEEE Photonics Technology Letters*, vol. 27, pp. 1795, 2015.  
<https://doi.org/10.1109/LPT.2015.2439576>
- [P11] **J. M. Serres**, V. Jambunathan, X. Mateos, P. Loiko, A. Lucianetti, T. Mocek, K. Yumashev, V. Petrov, U. Griebner, M. Aguiló, and F. Díaz, “**Graphene Q-Switched Compact Yb:YAG Laser**,” *IEEE Photonics J.*, vol. 7, pp. 1, 2015.  
<https://doi.org/10.1109/JPHOT.2015.2476756>
- [P12] P. Loiko, **J. M. Serres**, X. Mateos, K. Yumashev, A. Yasukevich, V. Petrov, U. Griebner, M. Aguiló, and F. Díaz, “**Subnanosecond Tm:KLuW microchip laser Q-switched by a Cr:ZnS saturable absorber**,” *Opt. Lett.*, vol. 40, pp. 5220, 2015.  
<https://doi.org/10.1364/OL.40.005220>
- [P13] P. A. Loiko, **J. M. Serres**, X. Mateos, M. P. Demesh, A. S. Yasukevich, K. V. Yumashev, V. Petrov, U. Griebner, M. Aguiló, and F. Díaz, “**Spectroscopic and laser characterization of Yb,Tm: KLu(WO<sub>4</sub>)<sub>2</sub> crystal**,” *Opt. Mater.*, vol. 51, pp. 223, 2016.  
<https://doi.org/10.1016/j.optmat.2015.10.028>
- [P14] **J. M. Serres**, V. Jambunathan, P. Loiko, X. Mateos, H. Yu, H. Zhang, J. Liu, A. Lucianetti, T. Mocek, K. Yumashev, U. Griebner, V. Petrov, M. Aguiló, and F. Díaz, “**Microchip Laser Operation of Yb-Doped Gallium Garnets**,” *Opt. Mater. Express*, vol. 6, pp. 46, 2015.  
<https://doi.org/10.1364/OME.6.000046>
-

- [P15] **J. M. Serres**, P. Loiko, X. Mateos, V. Jambunathan, K. Yumashev, U. Griebner, V. Petrov, M. Aguiló, and F. Díaz, “**Q-switching of a Tm,Ho:KLu(WO<sub>4</sub>)<sub>2</sub> microchip laser by a graphene-based saturable absorber**,” *Laser Phys. Lett.*, vol. 13, pp. 025801, 2016.  
<https://doi.org/10.1088/1612-2011/13/2/025801>
- [P16] **J. M. Serres**, P. Loiko, X. Mateos, H. Yu, H. Zhang, J. Liu, K. Yumashev, U. Griebner, V. Petrov, M. Aguiló, and F. Díaz, “**Q-switching of Yb:YGG, Yb:LuGG and Yb:CNGG lasers by a graphene saturable absorber**,” *Opt. Quantum Electron.*, vol. 48, pp. 197, 2016.  
<https://doi.org/10.1007/s11082-016-0473-6>
- [P17] P. A. Loiko, **J. M. Serres**, X. Mateos, J. Liu, H. Zhang, A. S. Yasukevich, K. V. Yumashev, V. Petrov, U. Griebner, M. Aguiló, and F. Díaz, “**Passive Q-switching of Yb bulk lasers by a graphene saturable absorber**,” *Appl. Phys. B*, vol. 122, pp. 105, 2016.  
<https://doi.org/10.1007/s00340-016-6384-1>
- [P18] P. Loiko, **J.M. Serres**, X. Mateos, H. Yu, H. Zhang, J. Liu, K. Yumashev, U. Griebner, V. Petrov, M. Aguiló and F. Díaz, “**Thermal Lensing and Multiwatt Microchip Laser Operation of Yb:YCOB Crystals**,” in *IEEE Photonics Journal*, vol. 8, pp. 1, 2016.  
<https://doi.org/10.1109/JPHOT.2016.2555584>
- [P19] **J. M. Serres**, P. Loiko, X. Mateos, V. Jambunathan, A. S. Yasukevich, K. V. Yumashev, V. Petrov, U. Griebner, M. Aguiló, and F. Díaz, “**Passive Q-switching of a Tm,Ho:KLu(WO<sub>4</sub>)<sub>2</sub> microchip laser by a Cr:ZnS saturable absorber**,” *Appl. Opt.*, vol. 55, pp. 3757, 2016.  
<https://doi.org/10.1364/AO.55.003757>
- [P20] P. Loiko, **J. M. Serres**, X. Mateos, K. Yumashev, A. Yasukevich, V. Petrov, U. Griebner, M. Aguiló, and F. Díaz, “**Sub-nanosecond Yb:KLu(WO<sub>4</sub>)<sub>2</sub> microchip laser**,” *Opt. Lett.*, vol. 41, pp. 2620, 2016.  
<https://doi.org/10.1364/OL.41.002620>
- [P21] P. Loiko, S.J. Yoon, **J.M. Serres**, X. Mateos, S.J. Beecher, R.B. Birch, V.G. Savitski, A.J. Kemp, K. Yumashev, U. Griebner, V. Petrov, M. Aguiló, F. Díaz, and J.I. Mackenzie, “**Temperature-dependent spectroscopy and microchip laser operation of Nd:KGd(WO<sub>4</sub>)<sub>2</sub>**,” *Opt. Mater.*, vol. 58, pp. 365, 2016.  
<https://doi.org/10.1016/j.optmat.2016.06.005>
- [P22] V. Jambunathan, X. Mateos, P.A. Loiko, **J.M. Serres**, U. Griebner, V. Petrov, K.V. Yumashev, M. Aguiló, F. Díaz, “**Growth, spectroscopy and laser operation of Ho:KY(WO<sub>4</sub>)<sub>2</sub>**,” *J. Lumin.*, vol. 179, pp. 50, 2016.  
<https://doi.org/10.1016/j.jlumin.2016.06.049>
-

- 
- [P23] **J. M. Serres**, P. Loiko, X. Mateos, H. Yu, H. Zhang, Y. Chen, V. Petrov, U. Griebner, K. Yumashev, M. Aguiló, and F. Díaz, “**MoS<sub>2</sub> Saturable Absorber for Passive Q-Switching of Yb and Tm Microchip Lasers**,” *Opt. Mater. Express*, vol. 6, pp. 3262, 2016.  
<https://doi.org/10.1364/OME.6.003262>
- [P24] P. Loiko, X. Mateos, S. Y. Choi, F. Rottermund, **J. M. Serres**, M. Aguiló, F. Díaz, K. Yumashev, U. Griebner, and V. Petrov, “**Vibronic Thulium Laser at 2131 nm Q-switched by Single-Walled Carbon Nanotubes**,” *J. Opt. Soc. Amer. B, JOSA B*, vol. 33, pp. D19, 2016.  
<https://doi.org/10.1364/JOSAB.33.000D19>
- [P25] **J. M. Serres**, X. Mateos, P. Loiko, U. Griebner, V. Petrov, K. Yumashev, M. Aguiló, and F. Díaz, “**Indium-modified Yb:KLu(WO<sub>4</sub>)<sub>2</sub> crystal: Growth, spectroscopy and laser operation**,” *J. Lumin.* vol. 183, pp. 391, 2017.  
<https://doi.org/10.1016/j.jlumin.2016.11.018>
- [P26] X. Mateos, P. Loiko, **J. M. Serres**, K. Yumashev, U. Griebner, V. Petrov, M. Aguiló, and F. Díaz, “**Efficient Mico-Lasers Based on Highly Doped Monoclinic Double Tungstates**,” *IEEE Journal of Quantum Electronics*, vol. 53, pp. 1, 2017.  
<https://doi.org/10.1109/JQE.2017.2681626>
- [P27] A.S. Yasukevich, P. Loiko, N.V. Gusakova, **J. M. Serres**, X. Mateos, K.V. Yumashev, N.V. Kuleshov, V. Petrov, U. Griebner, M. Aguiló, and F. Díaz, “**Modelling of graphene Q-switched Tm lasers**,” *Opt. Commun.*, vol. 389, pp. 15, 2017.  
<https://doi.org/10.1016/j.optcom.2016.12.023>
- [P28] **J. M. Serres**, X. Mateos, P. Loiko, J. Rosell-Llompart, L. B. Modesto-López, K. Yumashev, U. Griebner, V. Petrov, J. J. Carvajal, M. Aguiló, and F. Díaz, “**Oriented Single-Walled Carbon Nanotubes in polymer fibres; Characterization and laser application as a Saturable Absorber**,” in preparation.
- [P29] L. Z. Zhang, Z. B. Lin, H.F. Lin, G. Zhang, X. Mateos, P. Loiko, **J. M. Serres**, M. Aguiló, and F. Díaz, Y.C. Wang, V. Petrov, U. Griebner, E. Vilejshikova, K. Yumashev, and W. D. Chen “**Crystal growth, optical spectroscopy and laser action of Tm<sup>3+</sup> -doped monoclinic magnesium tungstate**,” *Opt. Express*, vol. 25, pp. 3682, 2017.  
<https://doi.org/10.1364/OE.25.003682>
- [P30] P. Loiko, **J. M. Serres**, X. Mateos, P. Koopmann, K. Yumashev, M. Aguiló, F. Díaz, U. Griebner, V. Petrov, and C. Kränkel, “**Highly- efficient Tm<sup>3+</sup>:RE<sub>2</sub>O<sub>3</sub> sesquioxide microchip lasers based on thermal guiding**,” to be submitted to *Opt. Mater. Express*.
-

- [P31] R. Lan, X. Mateos, Y. Wang, **J. M. Serres**, P. Loiko, J. Li, Y. Pan, U. Griebner, and V. Petrov, “**Semiconductor saturable absorber Q-Switching of a holmium micro-laser,**” Opt. Express, vol. 25, pp. 4579, 2017.  
<https://doi.org/10.1364/OE.25.004579>
- [P32] P. Loiko, **J. M. Serres**, X. Mateos, S. Tacchini, M. Tonelli, S. Veronesi, D. Parisi, A. Di Lieto K. Yumashev, U. Griebner, and V. Petrov, “**Comparative spectroscopy and thermo-optics study of Tm:LiLnF<sub>4</sub> (Ln=Y, Gd, and Lu) crystals for highly-efficient microchip lasers at ~2μm,**” Opt. Mater. Express, vol. 7, pp. 844, 2017.  
<https://doi.org/10.1364/OME.7.000844>
- [P33] P. Loiko, **J. M. Serres**, X. Mateos, L. Z. Zhang, Z. B. Lin, H. F. Lin, G. Zhang, S. Y. Choi, F. Rotermunf, V. Petrov, U. Griebner, Y.C. Wang, M. Aguiló, F. Díaz, and W. Chen, “**Monoclinic Tm<sup>3+</sup>:MgWO<sub>4</sub>: A promising crystal for continuous-wave and passively Q-switched laser at ~ 2μm,**” Opt. Lett. vol. 42, pp. 1177, 2017.  
<https://doi.org/10.1364/OL.42.001177>

Other results obtained during this thesis but not directly related to the study, all of which have been published in **indexed international journals**:

- [OP1] P. A. Loiko, V. I. Dashkevich, S. N. Bagaev, V. A. Orlovich, X. Mateos, **J. M. Serres**, E. V. Vilejshikova, A. S. Yasukevich, K. V. Yumashev, N. V. Kuleshov, E. B. Dunina, A. A. Kornienko, S. M. Vatnik, and A. A. Pavlyuk, "**Judd–Ofelt analysis of spectroscopic properties of  $\text{Eu}^{3+}:\text{KLu}(\text{WO}_4)_2$  crystal,**" J. Lumin., vol. 168, pp. 102, 2015.
- [OP2] P. A. Loiko, E. V. Vilejshikova, X. Mateos, **J. M. Serres**, V. I. Dashkevich, V. A. Orlovich, A. S. Yasukevich, N. V. Kuleshov, K. V. Yumashev, S. V. Grigoriev, S. M. Vatnik, S. N. Bagaev, and A. A. Pavlyuk, "**Spectroscopy of tetragonal  $\text{Eu}:\text{NaGd}(\text{WO}_4)_2$  crystal,**" Opt. Mater., vol. 57, pp. 1, 2016.
- [OP3] P. Loiko, E. Vilejshikova, X. Mateos, **J. M. Serres**, E. Dunina, A. Kornienko, K. Yumashev, M. Aguiló, F. Díaz, "**Europium doping in monoclinic  $\text{KYb}(\text{WO}_4)_2$  crystal,**" J. Lumin, vol. 183, pp. 217, 2017.
- [OP4] A. P. Voitovich, P. A. Loiko, X. Mateos, L. P. Runets, **J. M. Serres**, and A. P. Stupak, "**Nanosized clusters in subsurface layers of lithium fluoride and their influence on photoluminescence properties of radiation-induced color centers,**" J. Lumin., vol. 188, pp. 75, 2017.
- [OP5] Zhu Zhang, Pavel Loiko, Xavier Mateos, **Josep maria Serres**, Francesc Díaz, Magdalena Aguiló, Weidong Chen, Elena Vilejshikova, Konstantin Yumashev, Uwe Griebner, Valentin Petrov, and Zhoubin Lin, "**Disordered  $\text{Tm}:\text{Ca}_9\text{La}(\text{VO}_4)_7$ : Novel potential crystal for tunable lasers,**" Opt. Mater. Express, vol. 7, no. 2, pp. 484, 2017.

List of publications for international/ national conferences related to the results of this thesis, in chronological order:

- [C1] P.A. Loiko, **J.M. Serres**, X. Mateos, K.V. Yumashev, N.V. Kuleshov, V. Petrov, U. Griebner, M. Aguiló and F. Díaz, **“Thermal Lensing in Tm:KLu(WO<sub>4</sub>)<sub>2</sub> Laser Crystals Cut Along the Optical Indicatrix Axes,”** Europhoton (*Neuchatel, Switzerland, 24-29 August 2014*)
- [C2] **Josep Maria Serres**, Xavier Mateos, Pavel Loiko, Konstantin Yumashev, Nikolai Kuleshov, Valentin Petrov, Uwe Griebner, Magdalena Aguiló and Francesc Díaz, **“3.2 W output power of a diode-pumped Tm:KLu(WO<sub>4</sub>)<sub>2</sub> microchip laser,”** Europhoton (*Neuchatel, Switzerland, 24-29 August 2014*)
- [C3] **Josep M. Serres**, Xavier Mateos, Uwe Griebner, Valentin Petrov, Magdalena Aguiló and Francesc Díaz, **“Graphene Saturable Absorber Q-switched Tm:KLu(WO<sub>4</sub>)<sub>2</sub> Laser Emitting at 2 μm,”** ASSL (Shanghai, China, 16–21 November 2014)
- [C4] Xavier Mateos, Pavel Loiko, **Josep Maria Serres**, Konstantin Yumashev, Alexander Malyarevich, Alexei Onushchenko, Valentin Petrov, Uwe Griebner, Magdalena Aguiló, and Francesc Díaz, **“Inband-Pumped Ho:KLu(WO<sub>4</sub>)<sub>2</sub> Microchip Laser Q-switched with a PbS-Quantum-Dot-Doped Glass,”** CLEO USA (San Jose, California, USA, 10-15 May 2015)
- [C5] Xavier Mateos, **Josep Maria Serres**, Pavel Loiko, Konstantin Yumashev, Valentin Petrov, Uwe Griebner, Magdalena Aguiló, and Francesc Díaz, **“Graphene-Based Saturable Absorber for Passive Q-switching of Tm:KLu(WO<sub>4</sub>)<sub>2</sub> Microchip Laser,”** CLEO USA (San Jose, California, USA, 10-15 May 2015)
- [C6] **Josep Maria Serres**, Venkatesan Jambunathan, Antonio Lucianetti, Tomas Mocek, Xavier Mateos, Pavel Loiko, Konstantin Yumashev, Valentin Petrov, Uwe Griebner, Magdalena Aguiló and Francesc Díaz, **“Graphene-Based Q-Switching of a Compact Passively-Cooled Yb:YAG Laser,”** CLEO Europe (Munich, Germany, 21-25 June 2015)
- [C7] **Josep Maria Serres**, Xavier Mateos, Pavel Loiko, Venkatesan Jambunathan, Konstantin Yumashev, Valentin Petrov, Uwe Griebner, Magdalena Aguiló and Francesc Díaz, **“Q-switching of a Tm,Ho:KLu(WO<sub>4</sub>)<sub>2</sub> Microchip Laser at 2061 nm by a Graphene-Based Saturable Absorber,”** CLEO Europe (Munich, Germany, 21-25 June 2015)
- [C8] Pavel Loiko, **Josep Maria Serres**, Xavier Mateos, Konstantin Yumashev, Nikolai Kuleshov, Valentin Petrov, Uwe Griebner, Magdalena Aguiló and Francesc Díaz, **“Vibronic 2.1 μm Yb,Tm:KLu(WO<sub>4</sub>)<sub>2</sub> Microchip Laser,”** CLEO Europe (Munich, Germany, 21-25 June 2015)
- [C9] Pavel Loiko, **Josep Maria Serres**, Xavier Mateos, Venkatesan Jambunathan, Konstantin Yumashev, Valentin Petrov, Uwe Griebner, Magdalena Aguiló and Francesc Díaz, **“Passive Q-switching and Self-Raman Conversion in Yb:KLu(WO<sub>4</sub>)<sub>2</sub> Microchip Laser,”** CLEO Europe (Munich, Germany, 21-25 June 2015)

- [C10] Xavier Mateos, Josep Maria Serres, Pavel Loiko, Konstantin Yumashev, Nikolai Kuleshov, Valentin Petrov, Uwe Griebner, Magdalena Aguiló, and Francesc Díaz, **“Monoclinic Double Tungstate Microchip Lasers at 1 and 2  $\mu\text{m}$ ,”** CLEO Europe (Munich, Germany, 21-25 June 2015)
- [C11] J. M. Serres, X. Mateos, P. Loiko, K. Yumashev, N. Kuleshov, V. Petrov, U. Griebner, M. Aguiló and F. Díaz, **“Intracavity-Pumped Ho:KLu(WO<sub>4</sub>)<sub>2</sub> Microchip Laser at 2.1  $\mu\text{m}$ ,”** CLEO Pacific Rim (Busan, Korea, 24-28 August 2015)
- [C12] P. Loiko, J. M. Serres, X. Mateos, K. Yumashev, V. Petrov, U. Griebner, M. Aguiló and F. Díaz, **“Tm,Ho:KLu(WO<sub>4</sub>)<sub>2</sub> Microchip Laser Q-switched by a Cr<sup>2+</sup>:ZnS Saturable Absorber,”** CLEO Pacific Rim (Busan, Korea, 24-28 August 2015)
- [C13] J. M. Serres, P. Loiko, X. Mateos, K. Yumashev, V. Petrov, U. Griebner, M. Aguiló and F. Díaz, **“Q-switching of Yb:KLu(WO<sub>4</sub>)<sub>2</sub> Lasers with Graphene Saturable Absorbers,”** CLEO Pacific Rim (Busan, Korea, 24-28 August 2015)
- [C14] X. Mateos, J.M. Serres, P. Loiko, K. Yumashev, V. Petrov, U. Griebner, M. Aguiló and F. Díaz, **“Q-switched microchip lasers at 2  $\mu\text{m}$ ,”** ALT Portugal (Portugal, 7-11 September 2015)
- [C15] X. Mateos, J.M. Serres, P. Loiko, Haohai Yu, Huaijin Zhang, Junhai Liu, K. Yumashev, U. Griebner, V. Petrov, M. Aguiló and Fr. Díaz, **“Q-switching of Yb:YGG, Yb:LuGG and Yb:CNGG laser by a graphene saturable absorber,”** ALT Portugal (Portugal, 7-11 September 2015)
- [C16] Josep Maria Serres, Venkatesan Jambunathan, Pavel Loiko, Xavier Mateos, Haohai Yu, Huaijin Zhang, Junhai Liu, Antonio Lucianetti, Tomas Mocek, Konstantin Yumashev, Uwe Griebner, Valentin Petrov, Magdalena Aguiló and Francesc Díaz, **“Microchip Laser Operation of Yb-Doped Gallium Garnets,”** ASSL (Berlin, Germany, 04-09 October 2015)
- [C17] Josep Maria Serres, Xavier Mateos, Pavel Loiko, Joan Rosell-Llompart, Luis Balam Modesto-López, Konstantin Yumashev, Uwe Griebner, Valentin Petrov, Joan Josep Carvajal, Magdalena Aguiló and Francesc Díaz, **“Oriented Single-Walled Carbon Nanotubes as Saturable Absorber for Passive Q-Switching of a Tm:KLuW Microchip Laser,”** ASSL (Berlin, Germany, 04-09 October 2015)
- [C18] Pavel Loiko, Josep Maria Serres, Xavier Mateos, Konstantin Yumashev, Anatoly Yasukevich, Uwe Griebner, Valentin Petrov, Magdalena Aguiló and Francesc Díaz, **“Sub-nanosecond Tm:KLuW Microchip Laser Q-switched by a Cr:ZnS Saturable Absorber,”** ASSL (Berlin, Germany, 04-09 October 2015)
- [C19] Xavier Mateos, Josep Maria Serres, Pavel Loiko, Haohai Yu, Huaijin Zhang, Junhai Liu, Konstantin V. Yumashev, Uwe Griebner, Valentin Petrov, Magdalena Aguiló and Francesc Díaz, **“Microchip Laser Operation of Yb:YCOB Crystals,”** ASSL (Germany, 04-09 October 2015)
- [C20] Pavel Loiko, Xavier Mateos, Sun Young Choi, Fabian Rottermund, Josep Maria Serres, Magdalena Aguiló, Francesc Díaz, Konstantin V. Yumashev, Uwe Griebner and Valentin Petrov, **“Vibronic Thulium Laser at 2131 nm Q-switched Single Wall Carbon Nanotubes,”** Compact Mid-Infrared Coherent Sources, MICS, (Long Beach, California, USA, 20-22 March 2016)

- 
- [C21] **Josep Maria Serres**, Xavier Mateos, Pavel Loiko, Haohai Yu, Huaijin Zhang, Yanxue Chen, Valentin Petrov, Uwe Griebner, Konstantin Yumashev, Magdalena Aguiló, and Francesc Díaz, **“MoS<sub>2</sub> Saturable Absorber for Passive Q-Switching of Yb and Tm Microchip Lasers,”** CLEO USA (San Jose, California, USA, 5-10 June 2016)
- [C22] **J. M. Serres**, R. Lan P. Loiko, X. Mateos, K. Yumashev, S. Y. Choi, M. H. Kim, F. Rotermund, H. Yu, H. Zhang, Y. Chen, M. Aguiló, F. Díaz, U. Griebner, and V. Petrov, **“Passive Q-switching of Ho:KLuW lasers at ~2.1 μm by novel nanostructured saturable absorbers,”** Europhoton, (Vienna, Austria, 21-25 August 2016)
- [C23] **J. M. Serres**, P. Loiko, X. Mateos, K. Yumashev, V. Petrov, U. Griebner, M. Aguiló, and F. Díaz, **“Highly efficient monoclinic double tungstate microchip lasers at ~1 and 2 μm,”** Europhoton, (Vienna, Austria, 21-25 August 2016)
- [C24] P. Loiko, **J. M. Serres**, X. Mateos, K. Yumashev, A. Yasukevich, V. Petrov, U. Griebner, M. Aguiló, and F. Díaz, **“Sub-nanosecond Yb:KLuW/Cr:YAG microchip laser,”** Europhoton, (Vienna, Austria, 21-25 August 2016)
- [C25] P. Pecker, L. Bohatý, C. Liebald, M. Peltz, S. Vernay, D. Rytz, P. Loiko, **J. M. Serres**, X. Mateos, K. Yumashev, Y. Wang, V. Petrov, and U. Griebner, **“Sellmeier equations for CaGdAlO<sub>4</sub> and CaYAlO<sub>4</sub> laser host crystals,”** Europhoton, (Vienna, Austria, 21-25 August 2016)
- [C26] P. Loiko, **J. M. Serres**, X. Mateos, K. Yumashev, V. Petrov, U. Griebner, M. Aguiló, F. Díaz, and C. Kränkel, **“Thermal lensing in cubic sesquioxides Tm:Lu<sub>2</sub>O<sub>3</sub>, Tm:Y<sub>2</sub>O<sub>3</sub> and Tm:Sc<sub>2</sub>O<sub>3</sub>,”** Europhoton, (Vienna, Austria, 21-25 August 2016)
- [C27] Ruijun Lan, Xavier Mateos, Yicheng Wang, Pavel Loiko, **Josep Maria Serres**, Jiang Li, Yubai Pan, Konstantin Yumashev, Valentin Petrov, and Uwe Griebner, **“Semiconductor Saturable Absorber Q-Switching of a Holmium Microchip Laser,”** ASSL (Boston, USA, 30 Oct. - 3 Nov. 2016)
- [C28] Xavier Mateos, Pavel Loiko, **Josep Maria Serres**, Simone Tacchini, Alberto di Lieto, Mauro Tonelli, Stefano Veronesi, Konstantin Yumashev, Uwe Griebner, and Valentin Petrov, **“Comparative Study of Tm:LiLnF<sub>4</sub> (Ln=Y, Gd, and Lu) Crystals for Microchip Lasers at ~2μm,”** ASSL (Boston, USA, 30 Oct. - 3 Nov. 2016)
- [C29] **Josep Maria Serres**, Pavel Loiko, Xavier Mateos, Junhai Liu, Huaijing Zhang, Konstantin Yumashev, Uwe Griebner, Valentin Petrov, Magdalena Aguiló and Francesc Díaz, **“Multi-watt passively Q-switched Yb:YAB/Cr:YAG microchip lasers,”** SPIE Photonics West (San Francisco, USA, 31 January-2 February 2017)
- [C30] Pavel Loiko, **Josep Maria Serres**, Xavier Mateos, Xiaodong Xu, Jun Xu, Konstantin Yumashev, Uwe Griebner, Valentin Petrov, Magdalena Aguiló, Francesc Díaz and Arkadi Major, **“Highly-efficient multi-watt Yb:CALGO and Yb:CALYO microchip lasers,”** SPIE Photonics West (San Francisco, USA, 31 January-2 February 2017)
- [C31] Xavier Mateos, **Josep Maria Serres**, Pavel Loiko, Konstantin Yumashev, Uwe Griebner, Valentin Petrov, Magdalena Aguiló and Francesc Díaz, **“Spectroscopy and laser operation of Indium-modified Yb:KLuW: A promising crystal for femtosecond lasers,”** SPIE Photonics West (San Francisco, USA, 31 January-2 February 2017)
-

- [C32] L. Z. Zhang, Z. B. Lin, X. Mateos, P. Loiko, **J. M. Serres**, Y. C. Wang, U. Griebner, V. Petrov, M. Aguiló, F. Díaz, E. Vilejshikova, K. Yumashev, H. F. Lin, G. Zhang, and W. Chen, **“Growth, Spectroscopy and laser Operation of a Novel Disordered Tetragonal Tungstate Crystal – Tm:NazLa<sub>4</sub>(WO<sub>4</sub>)<sub>7</sub>,”** Advanced Lasers and Photon Sources, ( Yokoham, Japan, 18 -21 April 2017)
- [C33] L. Z. Zhang, Z. B. Lin, H. F. Lin, G. Zhang, X. Mateos, P. Loiko, **J. M. Serres**, M. Aguiló, F. Díaz, Y. C. Wang, U. Griebner, V. Petrov, E. Vilejshikova, K. Yumashev, and W. D. Chen, **“Growth, Spectroscopy and Laser Operation of Tm-doped Monoclinic magnesium Tungstate (Tm:MgWO<sub>4</sub>),”** CLEO USA, (San Jose, USA, 16-18 May 2017)

UNIVERSITAT ROVIRA I VIRGILI  
CONTINUOUS-WAVE AND PASSIVELY Q-SWITCHED SOLID-STATE MICROCHIP LASERS IN THE NEAR-INFRARED  
Josep Maria Serres Serres

UNIVERSITAT ROVIRA I VIRGILI  
CONTINUOUS-WAVE AND PASSIVELY Q-SWITCHED SOLID-STATE MICROCHIP LASERS IN THE NEAR-INFRARED  
Josep Maria Serres Serres

UNIVERSITAT ROVIRA I VIRGILI

CONTINUOUS-WAVE AND PASSIVELY Q-SWITCHED SOLID-STATE MICROCHIP LASERS IN THE NEAR-INFRARED

Josep Maria Serres Serres



UNIVERSITAT  
ROVIRA i VIRGILI